GROUND STATE PROPERTIES OF A WEAKLY-BOUND THREE-BODY HALO SYSTEM

by

HAPPY LERATO VILAKAZI

submitted in accordance with the requirements for
the degree of

MASTER OF SCIENCE

in the subject

PHYSICS

at the

UNIVERSITY OF SOUTH AFRICA

SUPERVISOR: PROF B. MUKERU
CO-SUPERVISOR: PROF. M. L. LEKALA

JANUARY 2023

Dedication

To my late mom

© University of South Africa 2023

Acknowledgments

First and foremost I would like to thank the mighty God for giving me strength to complete this study.

Special thanks to the following people

- My supervisors, Prof B. Mukeru and Prof M.L. Lekala for expert advise on the topic, guidance during the study and lastly for being patient with me during my darkest hour.
- My peers at the department for assisting and teaching me to use miscellaneous tools like LateX,gnuplots and others.
- The Department of Physics at UNISA for financial support,
- My employer for allowing me to go on study leave during the course of the study.
- Lastly, My family and friends who were encouraging me to complete the dissertation

Declaration

I, Happy L. Vilakazi, declare that this dissertation titled, "GROUND STATE PROPERTIES OF A WEAKLY-BOUND THREE-BODY HALO SYSTEM" and the work presented in it are my own. I confirm that all sources used or quoted, have been acknoledged by means of a complete reference.

_____

Signature

Date: 24 January 2023

Mr Happy L. Vilakazi (Student Number: 57401403)

Summary

In this dissertation, we investigate the role of the nucleon-nucleon (nn) and three-body interactions on the ground-state structure of the $^{22}\mathrm{C} \longrightarrow {}^{20}\mathrm{C} + n + n$ borromean system. We start by outlining the theoretical formulation of a three-body bound-state problems, starting with the fundamentals of two-body bound and scattering states. The different steps leading to the transformation of the three-body Schrödinger equation into a one-dimensional set of coupled differential equations are shown. These equations are numerically solved to obtain the three-body ground-state binding energy. The analysis of the numerical results show that even in the absence of the nn interaction, the system remains bound, provided the three-body interaction becomes more attractive. Similarly, the system remains bound in the absence of the three-body interaction, provided the nn interaction becomes more attractive. The ground-state binding energy is also found to be a continuous function of the strengths and ranges of both interactions, meaning that when these parameters increase, the binding energy increases as well, making the system to be more compact. The study presented in this dissertation highlights the interplay of the nn and three-body interactions in the dynamics of the three-body neutron-halo system. These results have been published in the Brazilian Journal of Physics (2022) **52**, 193. DOI: https://doi.org/10.1007/s13538-022-01194-5.

Using the ground-state binding energy, various thermodynamic properties such as the mean energy, the free energy, the entropy as well as the specific heat capacity of this system are also calculated.

Contents

© University of South Africa 2023

© University of South Africa 2023

List of Tables

© University of South Africa 2023

List of Figures

© University of South Africa 2023

Chapter 1

Introduction

Since the discovery of halo nuclei [1, 2], the study of the structure of these weakly-bound systems has attracted immense attention from both experimental and theoretical perspectives as exemplified by Refs. [3–32]. Quantum halos are generally regarded as systems with dominating few-body structure, with radii larger compared to the size of the classically allowed regions [2]. They are defined as a cloud of nucleons (the so-called core nucleus) to which one or two nucleons are weakly-bound, there the valence nucleon (s) being located in the state with low orbital angular momentum ($\ell \leq 1$), where ℓ is the orbital angular momentum of the core-nucleon(s) relative motion. Consequently, halo nuclei are identified as s-wave and p-wave systems, with relatively weak ground-state binding energy. The requirement of a lower ground-state orbital angular momentum is directed by the desire to minimize the centrifugal barrier, whose effect is to squeeze the valence nucleon closer to the core nucleus, hence preventing the formation of a halo state. As a results, most halo nuclei are s-wave systems, with $\ell = 0$ ground-state orbital angular momentum. Halo nuclei are grouped into two categories: neutron-halos (or neutron-rich systems, when the valence nucleon is a neutron), and proton-halo (neutron-rich systems, when the valence nucleon is proton). Due to the Coulomb barrier between the core nucleus and the valence proton, which prevents the latter from moving far away from the

© University of South Africa 2023

former, there are more neutron-halo systems than proton-halo ones. This is mainly attributed to the fact that there is no Coulomb barrier between the core nucleus and the valence neutron, since the latter is not charged.

Furthermore, halo nuclei can be categorized into two-body systems and three-body systems. A two-body halo system is obtained when only one nucleon is weakly-bound to the core nucleus. For example: $^{8}\mathrm{B} \rightarrow {}^{7}\mathrm{Be} + p$, $^{11}\mathrm{Be} \rightarrow {}^{10}\mathrm{Be} + n$, $^{15}\mathrm{C} \rightarrow {}^{14}\mathrm{C} + n$, $^{19}\mathrm{C} \rightarrow {}^{18}\mathrm{C} + n$, among others, where p, is the valence proton and n, the valence neutron. Due to advanced radioactive beam facilities, the neutron-rich limit of the nuclear chart for heavier nuclei is becoming more accessible, such that heavy neutron-halos are being identified (see for example Refs. [33–39]), whose internal structures are yet to be well understood. A three-body halo system is obtained when two nucleons are weakly-bound to the core nucleus. For example, $^{6}\mathrm{He} \rightarrow {}^{4}\mathrm{He} + n + n$, $^{11}\mathrm{Li} \rightarrow {}^{9}\mathrm{Li} + n + n$, $^{22}\mathrm{C} \rightarrow {}^{20}\mathrm{C} + n + n$, among others. A three-body halo system contains three two-body subsystems. For $^{6}\mathrm{He} \rightarrow {}^{4}\mathrm{He} + n + n$, these subsystems are $^{4}\mathrm{He} + n$, $n + {}^{4}\mathrm{He}$ and $n + n$. When none of the three subsystem is bound (which is the case for all three examples), the the system is called "Borromean" which is derived from Borromean rings, heraldic symbol of the Italian princes of Borromeo. The three rings are interlocked in such a way that if any of them breaks, the other two would also fall apart (see Fig.1.1). For example, $^{6}\mathrm{He} \rightarrow {}^{4}\mathrm{He} + n + n$ is a borromean system since none of the $^{4}\mathrm{He} + n$, $n + {}^{4}\mathrm{He}$ and $n + n$ two-body subsystems is bound. The chart in Figure 1.2, shows some of the well-known halo systems. A review on two-and three-body halo and other weakly-bound nuclear and atomic systems can be found in Ref. [2].

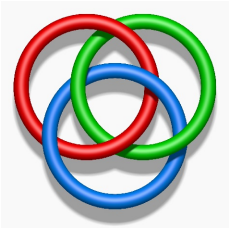

Figure 1.1: The Borromean rings illustrating three-body borromean systems.

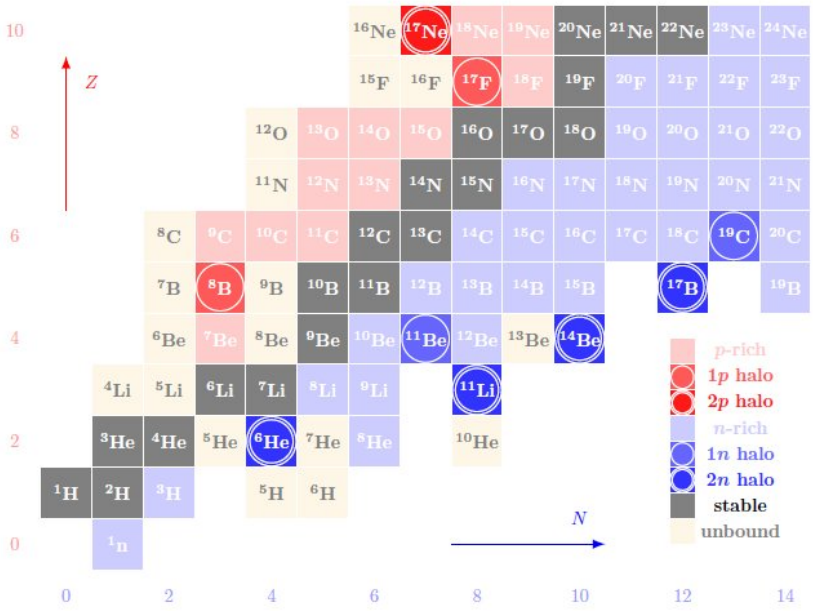

Figure 1.2: Nuclear chart of some of the known two-and three-body halo nuclei.

1.1 Problem statement

Despite these tremendous efforts, a complete understanding of the dynamics leading to the formation of a three-body system, remain an open problem. For example, the dynamics that an extra nucleon "brings" to an often unbound nucleus-nucleon two-body system to form a three-body system are some of the outstanding issues in this field. Furthermore, the literature still lacks a detailed analysis of the role of the

nucleon-nucleon (nn) and three-body interactions. For instance, what happens if the nn interaction is removed (switched off)? Will the system collapse? Which of the different interactions predominantly sustains a three-body system? Do the effects of the nn and three-body interactions depend on the size of the weakly-bound system? In other words, are these effects similar or different for ^{22}C and ^{6}He, sytems, where the former is about 3.7 times heavier than the latter? Naturally, one would assume that since a three-body system is formed by "adding" an extra nucleon to a two-body system, therefore, the nn interaction or nn correlations could be expected to play a dominant role, such that if this interaction is switched off, the whole system would collapse, as both nucleons could be flying independently outside the core nucleus. This assertion may be more plausible in the three-body borromean systems, where none of the three two-body subsystems is bound. However, few studies (if any) have been devoted to a careful analysis of the role of the nn interaction by considering the case where this interaction is removed from the three-body system.

Although it is asserted that the three-body interaction takes care of effects that are not explicitly accounted for by the two-body interactions [40–42], of the various interactions involved in a core$+n+n$ three-body system, it is the one that attracts the least attention. In most studies, the attention is focused on identifying new three-body halo candidate, leaving the impression that the role of the different interactions has been sufficiently elucidated. It could be that a more attractive three-body interaction may bind the three particles together even in the absence of a nn interaction. On the other hand, the range of the this interaction may turn out to be another important parameter in the study of three-body system. Among others, it can serve to further prove that indeed the two nucleons are well outside the core nucleus. For example, if the range of this interaction is shorter or equal to the radius of the core

nucleus, then the three-body system may not be expected to be bound, particularly in the case of a shallow nn interaction. This is because the two halo nucleons which are outside the core nucleus, will be out of the range of the three-body interaction. Therefore, studying the three-body binding energy as function of the range of the three-body interaction may to some extent, provide further insight in determining where exactly the two halo nucleons are located outside the core nucleus. It could also be that in the absence of a three-body interaction, a more attractive nn interaction might be needed in order to bind the three-body system. In the present study, we will consider all these aspects.

1.2 Aim and objective of the study

Owing to the complex dynamics involved in a three-body system, a detailed study of the nn and three-body interactions deserves further attention. In this paper, we present a detailed analysis of the role of the nn and three-body interactions on the ground-state structure of a three-body weakly-bound neutron-halo system. To this end, we will study the ground-state binding energy as function of the strength of the nn and three-body interactions, as well as the range of the three-body interaction. We will then perform several calculations by varying the depths of the nn and three-body interactions, and the range of the three-body interaction. Cases where the nn interaction and the three-body interaction are removed from the three-body system (of course not simultaneously), will also be considered. As a case study, we consider the ^{22}C three-body neutron-halo system. Although the exact ground-state binding energy of the former system is not well established (in Ref. [29], the 2003 mass evaluation gives a ground-state binding energy $S_{2n} = -0.4(8)\,\text{MeV}$. A 2012 direct mass measurement in Ref. [9], places a limit of $S_{2n} = -0.140(460)\,\text{MeV}$, and $S_{2n} =$

$-0.352\,\text{MeV}$ in the 2017 mass evaluation of Ref. [30]), it suffices to know that despite these discrepancies, the ^{22}C is bound and it is a borromean system. The interest in this system has drawn significant attention, as exemplified by Refs. [3–24]. On the other hand, the choice of this system is motivated by the fact that it is a neutron-halo system, meaning that we do not need to worry about the Coulomb interaction which would increase the number of potentials involved, which increases the number of free parameters. Our approach is to minimize the number of free parameters in order to facilitate our analysis. Furthermore, our study can be extended to weakly-bound heavy systems which are increasingly being identified [33–39].

Despite the spectacle progress in the study of the three-body weakly-bound systems, their thermodynamic properties have not yet attracted intense investigation, although there is an abundant literature on the thermodynamic properties of two-body atomic systems as evidenced by Refs. [43–55]. In this work, in an effort to contribute towards an investigation of the thermodyamic properties of the three-body weakly-bound systems, we will use the ground-state binding energy to calculate the ground-state thermodynamic properties. We will use this energy to calculate the profile function which we will obtain to calculate the ground-state mean energy, free energy, entropy as well as the specific heat capacity of the three-body system.

1.3 Methodological approach

In order to achieve the objectives assigned in this work, we will solve a three-body problem for bound-states. A direct solution of a Schrödinger equation that involves three-body particles does not exist even for bound-states. In this case, studies of three and more particles have resorted to approximate approaches. One of the most

popular approaches to the three-body systems is *Faddeev equations*, developed by L. D. Faddeev [56], and expanded to momentum space framework by Merkuriev and co-workers [57–61]. This approach is based on a decomposition of the three-body wave function into three two-body wave functions, the so-called *Faddeev amplitudes*, each of them associated with a two-body interaction. Upon the substitution of these amplitudes into the three-body Schrödinger equations, one obtains a set of three coupled differential equations which are numerically solved with the appropriate boundary conditions. However, each amplitude still contains a number of coordinates which complicates a numerical treatment of the problem, particularly for scattering states. As a result, further approximations of the Faddeev amplitudes have been applied, such as the total-angular momentum representation [62,63]. However, not only these amplitudes still depend on a number of coordinates, higher partial-waves are known to play an important role in the study of three-body weakly-bound systems. In order to circumvent this problem, most of studies of three-body weakly-bound systems have resorted to the hyperspherical harmonics method (HHM) [64–66].This method reduces the three-body Schödinger equation to a one-dimension radial coupled differential equations in the hyperradius (which is invariant under any permutation of the three particles). In this case, the asymptotic behavior of a three-body system in the hyperadius is similar to that of a two-body system, such that for a bound-state, the coupled differential equations are numerically solved with the same boundary conditions as a two-body system. This remarkable advantage makes the HHM the most popular method adopted to handle three-body systems, as evidenced by Refs. [1–42, 56–100]. In order to solve the coupled differential equations, the radial wave function is expanded on a basis of orthogonal polynomials such as the Lagrange polynomials [101], Laguerre Polynomials [102],among others,which exhibit nice con-

vergence behavior. In this dissertation, we also adopt the HHM in our investigation of the ground-state properties of the ^{22}C weakly-bound halo system.

1.4 Structure of the Dissertation

This dissertation is made up of five chapters. In Chapter 2, we discuss the basic formalism governing the dynamics of the two-body systems. Starting from the Schrödinger equation that describes the relative motion of two-body systems, we discuss the boundary conditions of bound states, scattering states as well as resonance states. The two-body potentials that are needed in the numerical solution of the Schrödinger are also discussed. Chapter 3, deals with the hyperspherical harmonics method for three-body systems. We first derive a complete basis hyperspherical harmonics on which the three-body wave function is expanded. The Faddeev equations are presented and the Faddeev amplitudes are expanded on the hyperspherical harmonics basis. The substitution of this expansion into Faddeev equations yields a one-dimensional set of coupled differential equations. The results are presented and discussed in Chapter 4, whereas our conclusion remarks are summized in Chapter 5.

Chapter 2

Fundamentals of two-body systems

In this chapter, we are discussing the basic formalism governing the dynamics of two-body systems. Starting from the Hamiltonian that describes the system, we are describing the corresponding Schrödinger equation as well as the wave function. The two-body interaction that enters this equation as an input in the numerical solution of this equation will be also discussed together with the boundary conditions. The chapter ends with a discussion of the two-body interactions that are useful in the numerical solution of the Schrödinger equation.

2.1 Two-body Schrödinger equation and wave function

In this section, we consider a two-body system, formed by a core nucleus "c", and a valence nucleon "v"(proton or neutron), which we we consider to be loosely bound to the core nucleus. We denote by $\boldsymbol{I}_c$, and $\boldsymbol{s}$ the spins of the core nucleus and nucleon respectively, and $\boldsymbol{x}$ their relative coordinate, associated with the orbital angular momentum $\boldsymbol{\ell}$. The core-nucleon relative motion is described by the following

Schrödinger equation

$$H_0\Phi(\boldsymbol{x}) = \varepsilon_{2b}\Phi(\boldsymbol{x}), \tag{2.1}$$

where $\Phi(\boldsymbol{x})$ is the wave function, ε_{2b} the total energy ($\varepsilon_{2b} < 0$) for bound-states and ($\varepsilon_{2b} > 0$) for scattering states, and H_0 the two-body Hamiltonian of given by

$$H_0 \;=\; \widehat{T}_{\boldsymbol{x}} + V_{cv}(x), \tag{2.2}$$

with $V_{cv}(x)$ is the core-nucleon interacting potential, and

$$\widehat{T}_{\boldsymbol{x}} = -\frac{\hbar^2}{2\mu_{cv}}\nabla^2_{\boldsymbol{x}} \tag{2.3}$$

is the kinetic energy operator, where μ_{cv} the reduced mass, given by

$$\mu_{cv} = \frac{m_c m_v}{m_c + m_v}, \tag{2.4}$$

(where m_c and m_v are the respective atomic masses of the core nucleus and the valence nucleon), and $\nabla^2_{\boldsymbol{x}}$ is the usual nabla operator. In spherical coordinates (x, θ, ϕ), the nabla operator is defined as

$$\begin{aligned}\nabla^2_{\boldsymbol{x}} &= \frac{1}{x^2}\frac{\partial}{\partial x}\left(x^2\frac{\partial}{\partial x}\right) + \frac{1}{x^2\sin^2\theta}\frac{\partial}{\partial\theta}\left(\sin\theta\frac{\partial}{\partial\theta}\right) + \frac{1}{x^2\sin^2\theta}\frac{\partial^2}{\partial\phi^2} \\ &= \frac{1}{x^2}\frac{\partial}{\partial x}\left(x^2\frac{\partial}{\partial x}\right) + \frac{\widehat{\boldsymbol{\ell}}^2}{x^2},\end{aligned} \tag{2.5}$$

where $\widehat{\boldsymbol{\ell}^2}$ is the orbital angular momentum operator, whose z-projection is

$$\widehat{\boldsymbol{\ell}}_z = \frac{\hbar}{i}\frac{\partial}{\partial\phi}. \tag{2.6}$$

With equation (2.5), the kinetic energy operator becomes

$$\widehat{T}_{\boldsymbol{x}} \;=\; -\frac{\hbar^2}{2\mu_{cv}}\left[\frac{1}{x^2}\frac{\partial}{\partial x}\left(x^2\frac{\partial}{\partial x}\right)+\frac{\widehat{\boldsymbol{\ell}^2}}{x^2}\right]. \tag{2.7}$$

Since we consider the potential $V_{cv}(x)$ to be spherical, the expression (2.5) ensures that the Hamiltonian H_0 commutes with the operators $\widehat{\boldsymbol{\ell}}$ and $\widehat{\boldsymbol{\ell}}_z$. To construct the wave function $\Phi(\boldsymbol{x})$, we need to consider the internal structures of both the core nucleus and valence nucleon. In this case, the wave function is written as follows

$$\Phi(\boldsymbol{x}) = i^{\ell}\Big[[Y_{\ell}^{\nu}(\Omega_{\boldsymbol{x}})\otimes\mathcal{X}_s^{\mu}]_{jm_j}\otimes\mathcal{X}_I^{\sigma}\Big]_{j_{ab}\Lambda}\frac{u_{\ell}^{j_{ab}}(k,x)}{x} \tag{2.8}$$

where $Y_{\ell}^{\nu}(\Omega_{\boldsymbol{x}})$ is the usual spherical harmonics (ν is the z-projection of the orbital angular momentum ℓ, $\Omega_{\boldsymbol{x}}\equiv(\theta_x,\phi_x)$ is a solid angle expression in terms of spherical coordinates), j is the total angular momentum obtained from the coupling of ℓ and s ($\boldsymbol{j}=\boldsymbol{\ell}+\boldsymbol{s}$), with m_j its z-projection, $\mathcal{X}_s^{\mu}$ is the nucleon spin wave function (μ is the z-projection of the spin s), ($m_j=\nu+\mu$), $\mathcal{X}_I^{\sigma}$ is the wave function of the spin of the core nucleus (σ is the z-projection of the spin I), j_{ab} is the total angular momentum obtained from the coupling of the angular momentum j and the spin I ($\boldsymbol{j}_{ab}=\boldsymbol{j}+\boldsymbol{I}$), and Λ is its z-projection ($\Lambda=m_j+\sigma$). In equation (2.8), we are assuming the $\boldsymbol{\ell}+\boldsymbol{s}$, $\boldsymbol{j}+\boldsymbol{I}=\boldsymbol{j}_{ab}$ coupling scheme, and $u_{\ell}^{j_{ab}}(k,x)$ is the radial wave function, with $k=\sqrt{\dfrac{2\mu_{cv}\varepsilon_{2b}}{\hbar^2}}$ the wave number. In what follows, we shall denote the wave function $\Phi(\boldsymbol{x})$ as $\Phi_{j_{ab}\Lambda}(\boldsymbol{x})$. Using the relation of angular momentum couplings

and to the Clebsh-Gorden coefficients, we can write equation (2.8) as follows

$$\Phi_{j_{ab}\Lambda}(\boldsymbol{x}) = i^{\ell}\sum_{\nu\mu}\sum_{m_j\sigma}\langle \ell\nu s\mu|jm_j\rangle\langle jmjI\sigma|j_{ab}\Lambda\rangle Y_{\ell}^{\nu}(\Omega_{\boldsymbol{x}})\mathcal{X}_{s}^{\mu}\mathcal{X}_{I}^{\sigma}\frac{u_{\ell}^{j}(k,x)}{x}, \tag{2.9}$$

where $\langle ....|..\rangle$ is the Clebsh-Gordon coefficient. If the spin of the core nucleus is zero ($I_c = 0$), then $j_{ab} = j$, and equation (2.9), reduces to

$$\Phi_{jm_j}(\boldsymbol{x}) = i^{\ell}\sum_{\nu\mu}\langle \ell\nu s\mu|jm_j\rangle Y_{\ell}^{\nu}(\Omega_{\boldsymbol{x}})\mathcal{X}_{s}^{\mu}\frac{u_{\ell}^{j}(k,x)}{x}. \tag{2.10}$$

It can be shown that the radial wave function (k, x) satisfies the following differential equation

$$\left[-\frac{\hbar^2}{2\mu_{cv}}\left(\frac{d^2}{dx^2} - \frac{\ell(\ell+1)}{x^2}\right) + V_{cv}(x)\right]u_{\ell}^{j}(k,r) = \varepsilon_{2b}u_{\ell}^{j}(k,x), \tag{2.11}$$

where $\ell(\ell+1)/x^2$ is known as the centrifugal barrier. For $\ell \neq 0$, it creates a strong repulsion at short distances, and pushes the wave function outside the area of closest approach. It is also one of the reasons halo states in neutron rich nuclei with $\ell \neq 0$ are unlikely.

2.2 Boundary conditions

In order to solve the differential equation (2.11), one needs to impose appropriate boundary conditions. For bound state, the boundary conditions require the wave function $u_{\ell}^{j}(k,x)$ to be regular at the origin $[u_{\ell_b}^{j_b}(k,x) \to 0, x \to 0]$, and the following

form at larger distance ($x \to \infty$)

$$u^{j_b}_{\ell_b}(k_b, x) \overset{x\to\infty}{\to} C_b W_{-\eta,\ell_b+\frac{1}{2}}(2k_b x), \tag{2.12}$$

where C_b is the asymptotic normalization coefficient (ANC), and $W_{-\eta,\ell_b+\frac{1}{2}}(2k_b x)$ ($\eta = \frac{\mu_{cv}}{\hbar^2}\frac{Z_c Z_v e^2}{k}$ is the Sommerfeld parameter, with $Z_c e$, $Z_v e$ are the core and nucleon charges, respectively) is the Whittaker function [103], having the following asymptotic form

$$W_{-\eta,\ell_b+\frac{1}{2}}(2k_b x) \overset{x\to\infty}{\to} e^{-k_I x+\eta_I \ln(2k_b x)}, \tag{2.13}$$

with

$$\eta_I = \frac{-iZ_c Z_v e^2 \mu_{cv}}{\hbar^2 k_b} \tag{2.14}$$

$$k_b = i\sqrt{\frac{2\mu_{cv}}{\hbar^2}E_b}, \tag{2.15}$$

where $\varepsilon_{2b} < 0$ is the binding energy. In this neutron case, $Z_v = 0$, such that equation (2.12) reduces to

$$u^{j_b}_{\ell_b}(k_b, x) \overset{x\to\infty}{\to} C_b e^{-k_b x}, \tag{2.16}$$

The bound-state wave function is square-integrable and is normalized according to

$$\int_0^\infty |u^{j_b}_{\ell_b}(k_b, x)|^2 = 1, \tag{2.17}$$

and fulfill the following orthogonality property

$$\left\langle u^{j_b}_{\ell_b}(k_b,x)|u^{j'_b}_{\ell'_b}(k'_b,x)\right\rangle = \delta_{\ell_b\ell'_b}\delta_{j_bj'_b}\delta_{k_bk'_b}, \tag{2.18}$$

where δ_r is the delta function [103]. For scattering states, the wave function $u^j_\ell(k,x)$ is also regular at the origin, and has the following behavior in the asymptotic region

$$u^j_\ell(k,x) \overset{x\to\infty}{\to} F_\ell(\eta,kx)\cos\delta_{\ell j}(k) + G_\ell(\eta,kx)\sin\delta_{\ell j}(k), \tag{2.19}$$

where $\delta_{\ell j}(k)$ are the nuclear phase shifts, and $F_\ell(\eta,kx)$ is the regular [$F_\ell(\eta,kx\to 0)\to 0$], and $G_\ell(\eta,kx)$ irregular [$G_\ell(\eta,kx\to 0)\neq 0$] Coulomb functions [104]. They exhibit the following asymptotic behaviour

$$\begin{aligned} F_\ell(\eta,kx) &\overset{x\to\infty}{\to} \sin\left[kx-\eta\ln(2kx)-\frac{\ell\pi}{2}+\sigma^\ell_\eta(k)\right], \\ G_\ell(\eta,kx) &\overset{x\to\infty}{\to} \cos\left[kx-\eta\ln(2kx)-\frac{\ell\pi}{2}+\sigma^\ell_\eta(k)\right], \end{aligned} \tag{2.20}$$

where $\sigma^\ell_\eta(k)$ are the Coulomb phases, given by

$$\sigma^\ell_\eta(k) = \arg\Gamma(1+\ell+i\eta), \tag{2.21}$$

with $\Gamma(y)$ the Gamma function. For a valence neutron, where $\eta=0$, the Coulomb functions transform into spherical Bessel functions $j_\ell(kx)$ and $n_\ell(kx)$, which in the

asymptotic region and are given by

$$\begin{aligned} j_\ell(kx) &\overset{x\to\infty}{\to} \sin\left(kx - \frac{\ell\pi}{2}\right), \\ n_\ell(kx) &\overset{x\to\infty}{\to} \cos\left(kx - \frac{\ell\pi}{2}\right), \end{aligned} \tag{2.22}$$

and they are generally defined as

$$\begin{aligned} j_\ell(kx) &= (-x)^\ell \left(\frac{1}{x}\frac{d}{dx}\right)^\ell \frac{\sin(x)}{x} \\ n_\ell(kx) &= -(-x)^\ell \left(\frac{1}{x}\frac{d}{dx}\right)^\ell \frac{\cos(x)}{x}. \end{aligned} \tag{2.23}$$

In this case, equation (2.19) becomes

$$u_\ell^j(k,x) \overset{x\to\infty}{\to} \sin\left(kx + \frac{\ell\pi}{2} + \delta_{\ell j}(k)\right). \tag{2.24}$$

Scattering wave functions are not square-integrable. they satisfy the following orthogonality relation

$$\left\langle u_\ell^j(k,x) | u_{\ell'}^{j'}(k,x) \right\rangle = \delta(k-k')\delta_{\ell\ell'}\delta_{jj'}, \tag{2.25}$$

and they are orthogonal to the bound states,

$$\left\langle u_\ell^j(k,x) | u_{\ell_b}^{j_b}(k_b,x) \right\rangle = 0. \tag{2.26}$$

The phase shifts $\delta_{\ell j}(k)$ can be used to define the parameters of a resonance state. A resonance is regarded as a "quasi-bound" short-lived state which happens when

the particle gets trapped in the Coulomb barrier for a while, and among others, it is characterized by the fact that the corresponding phase shift approaches $\pi/2$ as the incident energy approaches the resonance energy (ε_r). Its width Γ is given in terms of $\delta_{\ell j}(k)$ by

$$\Gamma = 2\left[\frac{\partial}{\partial\varepsilon}\cot\delta_{\ell j}\bigg|_{\varepsilon=\varepsilon_r}\right]^{-1}. \tag{2.27}$$

2.3 Two-body potentials

The important parameter that enters the Schrödinger equation is the interaction between the two particles. A bound-state and resonant state cannot exist unless the interacting potential exists. When this potential does no longer exist, the two particles are said to be in the continuum, where they are flying independently of each other. This is where the asymptotic behavior (2.19) of the scattering states applies. For bound-states, when the potential vanishes in the asymptotic region, the wave function decays to zero, since the system cannot be bound beyond the range of the potential. In general, the core-nucleon potential $V_{cv}(x)$ is given by

$$V_{cv}(x) = V_{cv}^{nucl}(x) + V_{cv}^{coul}(x) + V_{cent}(x), \tag{2.28}$$

where $V_{cv}^{nucl}(x)$ is the nuclear component, $V_{cv}^{coul}(x)$ the Coulomb component, and $V_{cent}(x)$ the centrifugal component. The nuclear potential contains two terms, the central term and the spin-orbit coupling term, i.e.,

$$V_{cv}^{nucl}(x) = V_0^{nucl}(x) + V_{so}^{nucl}(x), \tag{2.29}$$

where $V_0^{nucl}(x)$ is the central term, and $V_{so}^{nucl}(x)$ the spin-orbit coupling term. There are a number of shapes adopted in the literature for the nuclear potential. The most popular is the Woods-Saxon shape, where both terms are given by

$$\begin{aligned} V_0^{nucl}(x) &= \frac{V_0}{\left[1+\exp\left(\frac{x-R_0}{a_0}\right)\right]} \\ V_{so}^{nucl}(x) &= \left(\frac{\hbar}{m_\pi c}\right)^2 \frac{(\boldsymbol{\ell}\cdot\boldsymbol{s})}{x}\frac{d}{dx}\frac{V_{so}}{\left[1+\exp\left(\frac{x-R_{so}}{a_{so}}\right)\right]}, \end{aligned} \tag{2.30}$$

where $\left(\frac{\hbar}{m_\pi c}\right)^2 = 2\,\text{fm}$, V_0 and V_{so} are the depths of the central and spin-orbit couplings, respectively, and (R_y, a_y), $[y \equiv (0, so)]$ are the corresponding radius and diffuseness. In general, the radius R_y is given by $R_y = r_y(A_c^{1/3} + A_v^{1/3})$. But when $A_v = 1$ (for a nucleon), $R_y = r_y \times A_c^{1/3}$ is always considered, where $r_y \in [1, 2]$ is the distance of closest approach. The different parameters are adjusted to reproduce bound and scattering properties of the two-body system. Normally, they make the fitting easier, the parameters R_y and a_y are fixed and only V_0 and V_{so} are adjusted. Sometimes, the same parameters do not describe the sytem's ground-state and scattering states properties. In this case, it is common to use a depth V_0 that is partial-wave dependent (ℓ-dependent), i.e., V_0^ℓ. However, if the system has no known continuum structure, there is no need using V_0^ℓ. An accurate description of the two-body scattering states is of great importance in the analysis of three-body systems. Equation (2.30) shows that the nuclear potential has a short range. This means that $V_{cv}^{nucl}(x) \to 0$ when $x \geq R_y$. The negative sign before V_0 accounts for the attractive nature of the nuclear potential.

The Coulomb potential is often considered to be a point-like sphere such that

$$V_{cv}^{coul}(x) = \begin{cases} \frac{Z_c Z_v e^2}{R_C}\left(\frac{3}{2} - \frac{x^2}{2R_C^2}\right) & x \leq R_C \\ \\ \frac{Z_c Z_v e^2}{x} & x > R_C, \end{cases} \tag{2.31}$$

where R_C is the Coulomb radius, similar to R_y. When the valence nucleon is a neutron, $V_{cv}^{coul}(x) = 0$. The centrifugal component is given by

$$V_{cv}^{cent}(x) = \frac{\ell(\ell+1)}{x^2}. \tag{2.32}$$

For an s-wave state ($\ell = 0$), $V_{cv}^{cent}(r) = 0$. When the interacting partners are both nucleons, one potential $V_{cv}(x)$ becomes a nucleon-nucleon potential [$V_{nn}(x)$]. A number of such potentials are available in the literature. For example, one mentions the semi-realistic Gogny-Pires-Tourreil (GPT) potential [105]

$$\begin{aligned} V_{nn}(x) &= V_c^{\ell}(x) + V_{so}(x) + V_t(x) \\ &= \sum_{i=1}^{3} V_{ci}^{\ell} \exp\left[-\left(x/x_{ci}^{\ell}\right)^2\right] + V_{\rm so} \exp\left[-\left(x/x_{so}\right)^2\right] \\ &+ \sum_{i=1}^{3} V_{ti} \exp\left[-\left(x/x_{ti}\right)^2\right], \end{aligned} \tag{2.33}$$

where $V_c^{\ell}(x)$ (which can also be ℓ-dependent) represents the central term, $V_{so}(x)$ the spin-orbit term and $V_t(x)$ the tensor term. More details of this potential can be found in Ref. [105] as well as the numerical values of the different parameters. Other nucleon-nucleon potentials are available in the liteturature, see for example

Refs. [85, 105–113]. All nn potentials are validated once they reproduce deuteron ($^2\mathrm{H} \to p + n$) ground and scattering properties, and other nn scattering properties. Another nn potential that is commonly used in the study of three-body system is given by the following simple Gaussian shape [114]

$$V_{nn}(x) = v_0 e^{(-x/x_0)^2}, \tag{2.34}$$

where $V_0 = -31.0\,\mathrm{MeV}$ and $x_0 = 1.8\,\mathrm{fm}$. These parameters reproduce the well-known nn scattering properties, such that nn the scattering length $a_s = -15\,\mathrm{fm}$.

Chapter 3

Formalism of three-body systems

In this chapter, we outline the main features of the hyperspherical harmonics method (HHM). Starting with the Jacobi coordinates, we will discuss the different expressions of the hyperspherical harmonics. We will separate the total wave function into its Faddeev amplitudes, which will be expanded on the hyperspherical harmonics basis. Once this expansion is substitued into the Schrödinger equation, a set of one-dimension coupled differential equations will be obtained. The three-body system we are interested in has the core "$c+n+n$", where "c" is the core nucleus surrounded by two weakly-bound neutrons "$n+n$". For the sake of simplicity, we will consider an inert core, meaning that we freeze its degrees of freedom, meaning that we do not consider the case where it is excited. We do not expect this approach to have any meaningful effect on the results, particularly when the core nucleus has no known excited bound-states, and is not deformed.

The spacial topology of the three-body system is represented by Fig.3.1. In that figure, we consider three particles i, j and k, where j identifies the core nucleus and i, k the two nucleons. In Fig.3.1, we identify the core nucleus by j and the two neutrons by i and k. In this case (j, k) is the interacting pair and i is the spectator particle. Fig.3.1b is obtained by a cyclic permutation of particles k and i, where

the (j,i) is the interacting pair and k the spectator particle. Fig.3.1c is obtained by a cyclic permutation of particles j and k, where (i,k) is the interacting pair and j the spectator particle. The three-body then corresponds to a set of three two-body subsystems, each interacting pair corresponds to a two-body potential.

3.1 Jacobi coordinates

Jacobi coordinates have the advantage of removing the center-of-mass motion when one is interested in the individual motion of each particle, making these coordinates attractive in various research fields. In Fig.3.1a, $(\boldsymbol{x}_i, \boldsymbol{y}_i)$ represents the Jacobi coordinates of the spectator particle i, $(\boldsymbol{x}_j, \boldsymbol{y}_j)$, represents the Jacobi coordinates of the spectator particle j, and $(\boldsymbol{x}_k, \boldsymbol{y}_k)$, the Jacobi coordinates of the spectator particle k. Considering A_i, A_j and A_k to be the atomic numbers of the particles i, j, and k, the Jacobi coordinates $(\boldsymbol{x}_i, \boldsymbol{y}_i)$ are defined as

$$\begin{aligned} \boldsymbol{x}_i &= \left(\frac{2A_jA_k}{A_i+A_j}\right)^{1/2}(\boldsymbol{r}_j - \boldsymbol{r}_k) \\ \boldsymbol{y}_i &= \left(\frac{2A_i(A_j+A_k)}{A_i+A_j+A_k}\right)^{1/2}\left(\boldsymbol{r}_i - \frac{A_j\boldsymbol{r}_j + A_k\boldsymbol{r}_k}{A_j+A_k}\right), \end{aligned} \tag{3.1}$$

where the vectors $\boldsymbol{r}_i$, $\boldsymbol{r}_j$ and $\boldsymbol{r}_k$ are space coordinates (internal coordinates) of the partices i, j and k. The other pair of coordinates $(\boldsymbol{x}_j, \boldsymbol{y}_j)$ and $(\boldsymbol{x}_k, \boldsymbol{y}_k)$, can be obtained from $(\boldsymbol{x}_i, \boldsymbol{y}_i)$ by applying the clockwise and anticlockwise permutation operators P^+

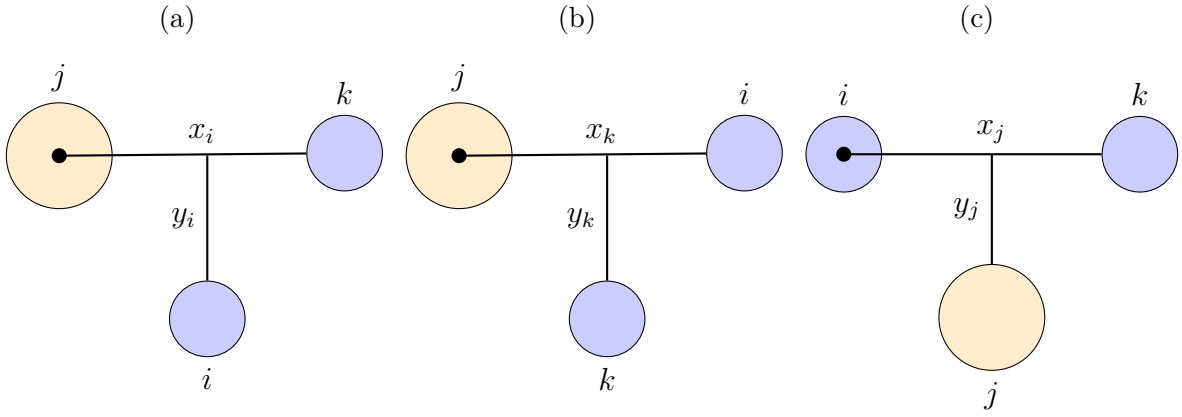

Figure 3.1: Jacobi coordinates for a three-body system

and P^-, as follows

$$\begin{pmatrix} \boldsymbol{x}_j \\ \boldsymbol{y}_j \end{pmatrix} = P^+ \begin{pmatrix} \boldsymbol{x}_i \\ \boldsymbol{y}_i \end{pmatrix}$$
$$\begin{pmatrix} \boldsymbol{x}_k \\ \boldsymbol{y}_k \end{pmatrix} = P^- \begin{pmatrix} \boldsymbol{x}_i \\ \boldsymbol{y}_i \end{pmatrix}, \tag{3.2}$$

where the operators P^+ and P^- are defined as

$$P^+ = \begin{bmatrix} \left(\frac{A_jA_k}{(A_j+A_i)(A_k+A_i)}\right)^{1/2} & -\left(\frac{AA_i}{(A_j+A_i)(A_k+A_i)}\right)^{1/2} \\ \left(\frac{AA_i}{(A_j+A_i)(A_i+A_k)}\right)^{1/2} & \left(\frac{A_jA_k}{(A_j+A_i)(A_k+A_i)}\right)^{1/2} \end{bmatrix}$$

$$P^- = \begin{bmatrix} \left(\frac{A_jA_k}{(A_j+A_i)(A_k+A_i)}\right)^{1/2} & \left(\frac{AA_i}{(A_j+A_i)(A_k+A_i)}\right)^{1/2} \\ -\left(\frac{AA_i}{(A_j+A_i)(A_k+A_i)}\right)^{1/2} & \left(\frac{A_jA_k}{(A_j+A_i)(A_k+A_i)}\right)^{1/2} \end{bmatrix}, \tag{3.3}$$

with $A = A_i + A_j + A_k$. In our case, where the particles i and j are nucleons ($A_i = A_j = 1$), these permutations become,

$$P^+ = \begin{pmatrix} \sqrt{\frac{A_k}{2A_k+2}} & -\sqrt{\frac{A_k+2}{2A_k+2}} \\ \sqrt{\frac{A_k+2}{2A_k+2}} & \sqrt{\frac{A_k}{2A_k+2}} \end{pmatrix}$$

$$P^- = \begin{pmatrix} \sqrt{\frac{A_k}{2A_k+2}} & \sqrt{\frac{A_k+2}{2A_k+2}} \\ -\sqrt{\frac{A_k+2}{2A_k+2}} & \sqrt{\frac{A_k}{2A_k+2}} \end{pmatrix}. \tag{3.4}$$

The coordinates $\boldsymbol{x}_j, \boldsymbol{y}_j$ and $\boldsymbol{x}_k, \boldsymbol{y}_k$ are then given by

$$\begin{aligned} \boldsymbol{x}_j &= \sqrt{\frac{A_k}{2A_k+2}}\boldsymbol{x}_i - \sqrt{\frac{A_k+2}{2A_k+2}}\boldsymbol{y}_i \\ \boldsymbol{y}_j &= \sqrt{\frac{A_k+2}{2A_k+2}}\boldsymbol{x}_i + \sqrt{\frac{A_i}{2A_i+2}}\boldsymbol{y}_i, \end{aligned} \tag{3.5}$$

and

$$\begin{aligned} \boldsymbol{x}_k &= \sqrt{\frac{A_k}{2A_k+2}}\boldsymbol{x}_i + \sqrt{\frac{A_k+2}{2A_k+2}}\boldsymbol{y}_i \\ \boldsymbol{y}_k &= -\sqrt{\frac{A_k+2}{2A_k+2}}\boldsymbol{x}_i + \sqrt{\frac{A_k}{2A_k+2}}\boldsymbol{y}_i, \end{aligned} \tag{3.6}$$

3.2 The angular momenta and spin of the system

Before we dive into the details of the HHM calculations, we would like to first outline the various ingredients. In particular, in this section, we would like to list the different angular momenta involved in the three-body system. In order to avoid cumbersome notations, we are dropping the subscipts on the Jacobi coordinates and simply refer to them as $\boldsymbol{x}$ and $\boldsymbol{y}$. The orbital angular momenta associated with the coordinates $\boldsymbol{x}$ and $\boldsymbol{y}$ are respectively $\boldsymbol{\ell}_x$ and $\boldsymbol{\ell}_y$, with m_x and m_y their corresponding z-projections. The orbital angular momenta $\boldsymbol{\ell}_x$ and $\boldsymbol{\ell}_y$ are coupled to obtain the total orbital angular momentum L ($\boldsymbol{L} = \boldsymbol{\ell}_x + \boldsymbol{\ell}_y$), with M_L its z-projection. The spins of the two nucleons are coupled to obtain the total spin S ($\boldsymbol{S} = \boldsymbol{s}_i + \boldsymbol{s}_k$), with M_S its z-projection. The orbital angular momentum $\boldsymbol{L}$ is coupled with the total spin $\boldsymbol{S}$ to obtain the angular momentum J_{ab} ($\boldsymbol{J}_{ab} = \boldsymbol{L} + \boldsymbol{S}$), with Λ its z-projection. The core spin will be identified by $\boldsymbol{I}$, with σ its z-projection. The coupling of the angular momentum $\boldsymbol{J}_{ab}$ with $\boldsymbol{I}$, gives the total angular momentum $\boldsymbol{J} = \boldsymbol{J}_{ab} + \boldsymbol{I}$, whose z-projection is M. This amounts to the following coupling scheme $\{\ [(\ell_x, \ell_y)L, (s_i, s_k)S]J_{ab}; I\}\ J$. For a core nucleus with zero spin, the couplings are significantly reduced and the coupling scheme reduces to $\{\ [(\ell_x, \ell_y)L, (s_i, s_k)S]\}\ J$. Other coupling scheme are possible and all of them are connected by the Raynal-Revai coefficients [115].

3.3 Hyperspherical Harmonics Method

3.3.1 Hyperspherical coordinates

Each Jacobi coordinate is defined in spherical coordinates by $\boldsymbol{x} \equiv (x, \theta_x, \phi_x) \equiv (x, \Omega_{\boldsymbol{x}})$, and $\boldsymbol{y} \equiv (y, \theta_y, \phi_y) \equiv (y, \Omega_{\boldsymbol{y}})$, where $\Omega_{\boldsymbol{x}}$ and $\Omega_{\boldsymbol{y}}$ are solid angles in the directions of the coordinates $\boldsymbol{x}$ and $\boldsymbol{y}$ expressed in spherical coordinates, and (x, y) are their radial components. The spherical harmonics associated with the solid angles $\Omega_{\boldsymbol{x}}$ and $\Omega_{\boldsymbol{y}}$ are denoted by $Y_{\ell_x}^{m_x}(\Omega_{\boldsymbol{x}})$ and $Y_{\ell_x}^{m_x}(\Omega_{\boldsymbol{y}})$, respectively. The angular part of the three-body wave function will then contain $\Omega \equiv (\Omega_{\boldsymbol{x}}, \Omega_{\boldsymbol{y}})$, which represents a set of four angles. The radial coordinates (x, y) are used to define the hyperspherical radial coordinate ρ, which is invariant under the permutation of the different Jacobi coordinates, and the hyperangle α. The set (ρ, α) represnts the hyperspherical coordinates and are defined as

$$\begin{aligned} \rho^2 &= x_i^2 + y_i^2 = x_j^2 + y_j^2 = x_k^2 + y_k^2 = \sum_{i=1}^{3} A_i r_i^2 \\ \alpha &= \arctan\left(\frac{x}{y}\right). \end{aligned} \tag{3.7}$$

In terms of the hyperspherical coordinates (ρ, α), the radial Jacobi coordinates x, y are given by

$$\begin{aligned} x &= \rho \cos\alpha \\ y &= \rho \sin\alpha. \end{aligned} \tag{3.8}$$

The three-body wave function denoted by $\Psi^{JM}(\boldsymbol{x}, \boldsymbol{y})$ is then a 6-dimension function, which can be factorized as $\Psi^{JM}(\boldsymbol{x}, \boldsymbol{y}) \equiv f(\rho) g(\Omega)$, where $f(\rho)$ represents its radial

part and $g(\Omega)$ its angular part, with $\Omega \equiv (\alpha, \Omega_{\boldsymbol{x}}, \Omega_{\boldsymbol{y}})$.

3.3.2 Hyperspherical Harmonics

Let $\mathcal{H}^{m_x,m_y}_{K\ell_x\ell_y}(\boldsymbol{x},\boldsymbol{y})$ be a homogeneous polynomial degree K (we will refer to K as the hypermomentum). A Harmonic Polynomial (HP), is homogeneous polynomial that satisfies the generalized Laplace equation [116]

$$\nabla^2 \mathcal{H}^{m_x m_y}_{K\ell_x\ell_y}(\boldsymbol{x},\boldsymbol{y}) \equiv \left(\frac{\partial^2}{\partial x^2} + \frac{\partial^2}{\partial y^2}\right)\mathcal{H}^{m_x m_y}_{K\ell_x\ell_y}(\boldsymbol{x},\boldsymbol{y}) \tag{3.9}$$

where the Laplacian ∇^2 is defined as

$$\nabla^2 = \frac{\partial^2}{\partial\rho^2} + \frac{5}{\rho}\frac{\partial}{\partial\rho} + \widehat{K}^2(\Omega), \tag{3.10}$$

where $\widehat{K}^2(\Omega)$ is the hyperangular momentum operator defined by

$$\widehat{K}^2(\Omega) = -\frac{\partial^2}{\partial\alpha^2} - 4\frac{\cos(2\alpha)}{\sin(2\alpha)}\frac{\partial}{\partial\alpha} + \frac{1}{\cos^2(\alpha)}\widehat{\ell}^2_x(\Omega_{\boldsymbol{x}}) + \frac{1}{\sin^2(\alpha)}\widehat{\ell}^2_y(\Omega_{\boldsymbol{y}}). \tag{3.11}$$

The hyperspherical Harmonics (HH), are the value of the HP at the surface of the unit hypersphere ($\rho = 1$), given by [117]

$$\mathscr{Y}^{\ell_x\ell_y}_{KLM_L}(\Omega) = \rho^{-K}\mathcal{H}^{m_x m_y}_{K\ell_x\ell_y}(\boldsymbol{x},\boldsymbol{y}), \tag{3.12}$$

and are eigenfunctions of $\widehat{K}$, implying that [116]

$$K^2(\Omega)\mathscr{Y}^{\ell_x\ell_y}_{KLM_L}(\Omega) = K(K+4)\mathscr{Y}^{\ell_x\ell_y}_{KLM_L}(\Omega). \tag{3.13}$$

They are also eigenfuctions of the square of the orbital angular momenta ℓ_x and ℓ_y, and their z-projections ℓ_{x_z} and ℓ_{y_z}, which means that

$$\begin{aligned}
\widehat{\ell}_x^2 \mathscr{Y}^{\ell_x\ell_y}_{KLM_L}(\Omega) &= \ell_x(\ell_x+1)\mathscr{Y}^{\ell_x\ell_y}_{KLM_L}(\Omega) \\
\widehat{\ell}_y^2 \mathscr{Y}^{\ell_x\ell_y}_{KLM_L}(\Omega) &= \ell_y(\ell_y+1)\mathscr{Y}^{\ell_x\ell_y}_{KLM_L}(\Omega) \\
\widehat{\ell}_{x_z} \mathscr{Y}^{\ell_x\ell_y}_{KLM_L}(\Omega) &= m_x\mathscr{Y}^{\ell_x\ell_y}_{KLM_L}(\Omega) \\
\widehat{\ell}_{y_z} \mathscr{Y}^{\ell_x\ell_y}_{KLM_L}(\Omega) &= m_y\mathscr{Y}^{\ell_x\ell_y}_{KLM_L}(\Omega).
\end{aligned} \tag{3.14}$$

In this case $\{\, \widehat{K}, \widehat{\ell}_x^2, \widehat{\ell}_y^2, \widehat{\ell}_{x_z}, \widehat{\ell}_{y_z}\}$, represents a complete set of observables in the three-body angular subspace, such that the HH define a complete and orthonormal basis on which the three-body wave function can be expanded. The HH are given by the following expression [86, 88, 118, 119]

$$\begin{aligned}
\mathscr{Y}^{\ell_x,\ell_y}_{KLM}(\Omega) &= [Y_{\ell_x}(\Omega_{\boldsymbol{x}}) \otimes Y_{\ell_y}(\Omega_{\boldsymbol{y}})]_{LM_L} \mathcal{P}_K^{\ell_x,\ell_y}(\alpha) \\
&= \sum_{m_x m_y} \langle \ell_x m_x \ell_y m_y | LM\rangle Y_{\ell_x}^{m_x}(\Omega_{\boldsymbol{x}}) Y_{\ell_y}^{m_y}(\Omega_{\boldsymbol{y}}) \mathcal{P}_K^{\ell_x,\ell_y}(\alpha),
\end{aligned} \tag{3.15}$$

where the function $\mathcal{P}_K^{\ell_x,\ell_y}(\alpha)$ is given by

$$\mathcal{P}_K^{\ell_x,\ell_y}(\alpha) = N_K^{\ell_x\ell_y} (\cos\alpha)^{\ell_x} (\sin\alpha)^{\ell_y} P_n^{(\ell_x+\frac{1}{2},\ell_y+\frac{1}{2})}(\cos 2\alpha), \tag{3.16}$$

with $P_n^{(a,b)}(z)$, being Jacobi polynomials, and $N_K^{\ell_x\ell_y}$ the normalization coefficients, defined as

$$N_K^{\ell_x\ell_y} = \left[\frac{2n!(K+2)(n+\ell_x+\ell_y+1)!}{\Gamma(n+\ell_x+\frac{3}{2})\Gamma(n+\ell_y+\frac{3}{2})}\right]^{1/2}, \tag{3.17}$$

where $n = \dfrac{K-\ell_x-\ell_y}{2}$, is a positive integer. The HH fulfil the following the orthogonality relation

$$\int d\Omega [\mathscr{Y}^{\ell_x,\ell_y}_{KLM_L}(\Omega)]^\star \times \mathscr{Y}^{\ell_x,\ell_y}_{KLM_L}(\Omega) = \delta_{KK'}\delta_{LL'}\delta_{\ell_x\ell'_x}\delta_{\ell_y\ell'_y}, \tag{3.18}$$

where $d\Omega = \sin^2\alpha\cos^2\alpha d\alpha d\Omega_{\boldsymbol{x}} d\Omega_{\boldsymbol{y}}$. The expansion of the three-body wave function on the HH basis is the foundation of the Hyperspherical Harmonics Expansion Method (HHEM) [86, 120]. If we consider the spins of the particles, the hyperspherical harmonics basis becomes

$$\mathscr{Y}^{JM}_{\gamma K}(\Omega) = \left[[\mathscr{Y}^{l_x,l_y}_{KLM_L}(\Omega) \otimes X_S]_{J_{ab}\Lambda} \otimes X_I \right]_{JM}, \tag{3.19}$$

where $\gamma \equiv \{\ [(\ell_x,\ell_y)L,(s_j,s_k)S_x]J_{ab};I\}$, represents the different quantum numbers, X_S and X_I are the spin wave functions. Equation (3.19) can be further expanded as follows

$$\begin{aligned} \mathscr{Y}^{JM}_{\gamma K}(\Omega) &= \sum_{m_{\ell_x}m_{\ell_y}} \langle \ell_x m_{\ell_x} \ell_y m_{\ell_y} | LM_L\rangle \sum_{M_L M_S} \langle LM_L SM_S | J_{ab}\Lambda\rangle \\ &\times \sum_{\Lambda\sigma} \langle J_{ab}\Lambda I\sigma | JM\rangle X_S X_I Y_{\ell_x}(\Omega_{\boldsymbol{x}}) Y_{\ell_y}(\Omega_{\boldsymbol{y}}) \mathcal{P}^{\ell_x,\ell_y}_K(\alpha). \end{aligned} \tag{3.20}$$

This equation reduces to

$$\begin{aligned} \mathscr{Y}^{JM}_{\gamma K}(\Omega) &= \sum_{m_{\ell_x}m_{\ell_y}} \langle \ell_x m_{\ell_x} \ell_y m_{\ell_y} | LM_L\rangle \sum_{M_L M_S} \langle LM_L SM_S | JM\rangle X_S \\ &\times Y_{\ell_x}(\Omega_{\boldsymbol{x}}) Y_{\ell_y}(\Omega_{\boldsymbol{y}}) \mathcal{P}^{\ell_x,\ell_y}_K(\alpha), \end{aligned} \tag{3.21}$$

if $I = 0$.

3.4 Faddeev Equations

Faddeev equations are known to be an accurate method that directly solve three-body problems, both for bound and scattering states. The essence of this method is the decomposition of the three-body wave function into its components, known as Faddeev amplitudes. In other words, each set of Jacobi coordinates $(\boldsymbol{x}, \boldsymbol{y})$ corresponds to one component of the total wave function, such that the total wave function contains three components. Before discussing these components, let us first write the three-body Schrödinger equation as follows

$$H_{3b}\Psi^{JM}(\boldsymbol{x}, \boldsymbol{y}) = \varepsilon_{3b}\Psi^{JM}, \tag{3.22}$$

where Ψ^{JM} is the three-body wave function, ε_{3b} is the total energy of the system, and H_{3b} is the Hamiltonian defined as

$$H_{3b} = H_0 + V_{ij}(x_k) + V_{ik}(x_j) + V_{jk}(x_i), \tag{3.23}$$

where H_0 is the Hamiltonian of the three free particles, and $V_{ij}(x_k)$, $V_{ik}(x_j)$ and $V_{jk}(x_i)$ are potentials of the interacting pairs (i, j), (i, k), and (j, k). Such potentials are discussed in section 2.28. The wave function $\Psi^{JM}(\boldsymbol{x}, \boldsymbol{y})$ is then decomposed into the following three components

$$\Psi^{JM}(\boldsymbol{x}, \boldsymbol{y}) \quad = \quad \psi_i^{JM}(\boldsymbol{x}_i, \boldsymbol{y}_i) + \psi_j^{JM}(\boldsymbol{x}_j, \boldsymbol{y}_j) + \psi_k^{JM}(\boldsymbol{x}_k, \boldsymbol{y}_k) \tag{3.24}$$

Inserting equations (3.24) and (3.23) into equation (3.22), one obtains the following set of coupled Faddeev equations

$$\begin{aligned}(H_0 + V_{ij}(x_k) - \varepsilon_{3b})\psi_k &= -V_{ij}(x_k)(\psi_j + \psi_i) \\ (H_0 + V_{ik}(x_j) - \varepsilon_{3b})\psi_j &= -V_{ik}(x_j)(\psi_k + \psi_i) \\ (H_0 + V_{jk}(x_i) - \varepsilon_{3b})\psi_i &= -V_{jk}(x_i)(\psi_i + \psi_k).\end{aligned} \tag{3.25}$$

These equations can be rewritten as

$$\begin{pmatrix} H_0 + V_{ij} - E_{3\mathrm{B}} & V_{ij} & V_{ij} \\ 0 & H_0 + V_{ik} - E_{3\mathrm{B}} & V_{ik} \\ 0 & 0 & H_0 + V_{jk} - E_{3\mathrm{B}} \end{pmatrix} \begin{pmatrix} \psi_k \\ \psi_j \\ \psi_i \end{pmatrix} = 0 \tag{3.26}$$

Because in our case the particles i and j are both nucleons, meaning that $V_{ik}(x_j) = V_{jk}(x_i)$, the above set of equations reduces to two equations,

$$\begin{aligned}(H_0 + V_{ij}(x_k) - \varepsilon_{3b})\psi_k &= -V_{ij}(P^+\psi_i + \psi_i) \\ (H_0 + V_{jk}(x_i) - \varepsilon_{3b})\psi_i &= -V_{jk}(x_j)(\psi_k + P^+\psi_i),\end{aligned} \tag{3.27}$$

where the operator P^+ is defined by equation (3.4).

3.4.1 Expansion of the wave function and coupled equations

In order to obtain a set of coupled differential equations to be solved numerically, we resort to the HHM and expand the Each Faddeev amplitude $\psi^{JM}(\boldsymbol{x}, \boldsymbol{y})$ on the

hyperspherical harmonics basis $\mathscr{Y}^{JM}_{\gamma K}(\Omega)$, as follows

$$\psi^{JM}(\boldsymbol{x},\boldsymbol{y}) = \rho^{-5/2}\sum_{\gamma K} F^{J}_{\gamma K}(\rho)\mathscr{Y}^{JM}_{\gamma K}(\Omega), \tag{3.28}$$

where $F^{J}_{\gamma K}(\rho)$ are the expansion coefficients to be deterimed numerically. The substitution of this expansion into the Schrödinger equation, yieds the following set of coupled differential equations

$$\left[-\frac{\hbar^2}{2m_N}\frac{d^2}{d\rho^2} + \mathscr{L}_K(\rho) - \varepsilon_{3b}\right]F^{J}_{\gamma K}(\rho) + \sum_{\gamma' K'} V^{J}_{\gamma' K',\gamma K}(\rho)F^{J}_{\gamma' K'}(\rho) = 0, \tag{3.29}$$

where m_N is the nucleon's mass, $\mathscr{L}_K(\rho)$ is given by

$$\mathscr{L}_K(\rho) = \frac{\hbar^2}{2m_N}\frac{(K+3/2)(K+5/2)}{\rho^2}, \tag{3.30}$$

and $V^{J}_{\gamma_i' K_i',\gamma_i K}(\rho)$, are coupling matrix elements, which contains three components each for each set of Jacobi coordinates, i.e.,

$$V^{J}_{\gamma' K',\gamma K}(\rho) = V^{J(i)}_{\gamma' K',\gamma K}(\rho) + V^{J(j)}_{\gamma' K',\gamma K}(\rho) + V^{J(k)}_{\gamma' K',\gamma K}(\rho), \tag{3.31}$$

The component $V^{J(i)}_{\gamma' K',\gamma K}(\rho)$ is given by

$$\begin{aligned} V^{J(i)}_{\gamma' K',\gamma K}(\rho) &= \langle \mathscr{Y}^{JM\star}_{\gamma' K'}(\Omega_i)|V_{jk}(x_i)|\mathscr{Y}^{JM}_{\gamma K}(\Omega_i)\rangle \\ &= \int \mathscr{Y}^{JM\star}_{\gamma' K'}(\Omega_i)V_{jk}(x_i)\mathscr{Y}^{JM}_{\gamma K}(\Omega_i)d\Omega_i. \end{aligned} \tag{3.32}$$

Again, for the sake of simplicity, we drop the subscripts i, j, k and rewrite this equation as

$$V^J_{\gamma' K', \gamma K}(\rho) = \int \mathscr{Y}^{JM\star}_{\gamma' K'}(\Omega) V(x) \mathscr{Y}^{JM}_{\gamma K}(\Omega) d\Omega, \tag{3.33}$$

where

$$d\Omega = \sin^2\alpha \cos^2\alpha d\alpha d\Omega_{\boldsymbol{x}} d\Omega_{\boldsymbol{y}}. \tag{3.34}$$

and the coordinate x is given in terms of the hyperspherical coordinates (ρ, α) by equation (3.8) Due to the orthoganality of the HH [equation (3.18)], and the following property of the spherical harmonics

$$\begin{aligned} \int d\Omega_{\boldsymbol{x}} Y^\star_{\ell_x}(\Omega_{\boldsymbol{x}}) Y_{\ell'_x}(\Omega_{\boldsymbol{x}}) &= \delta_{\ell_x \ell'_x} \\ \int d\Omega_{\boldsymbol{y}} Y^\star_{\ell_y}(\Omega_{\boldsymbol{y}}) Y_{\ell'_y}(\Omega_{\boldsymbol{y}}) &= \delta_{\ell_y \ell'_y}, \end{aligned} \tag{3.35}$$

and considering the potential $V(x)$ to be spherical, equation (3.33) becomes

$$V^J_{\gamma' K', \gamma K}(\rho) = \delta_{\gamma\gamma'}\delta_{KK'} \int_0^{\pi/2} \mathcal{P}^{\ell_x \ell_y}_K(\alpha) V(\rho\cos\alpha) \mathcal{P}^{\ell'_x \ell'_y}_{K'}(\alpha) \sin^2\alpha \cos^2\alpha d\alpha, \tag{3.36}$$

where the function $\mathcal{P}_K^{\ell_x \ell_y}(\alpha)$ is given by equation (3.16). Adopting the following change of variable

$$\begin{aligned} z &= \cos 2\alpha \\ \cos\alpha &= \left(\frac{1+z}{2}\right)^{1/2} \\ \sin\alpha &= \left(\frac{1-z}{2}\right)^{1/2} \\ dz &= -4\cos\alpha\sin\alpha d\alpha \\ d\alpha &= -\frac{dz}{4\cos\alpha\sin\alpha} = -\frac{dz}{4\left(\frac{1+z}{2}\right)^{1/2}\left(\frac{1-z}{2}\right)^{1/2}}, \end{aligned} \tag{3.37}$$

equation (3.34) becomes

$$\begin{aligned} d\Omega &= -\left(\frac{1+z}{2}\right)\left(\frac{1-z}{2}\right) \times \frac{dz}{4\left(\frac{1+z}{2}\right)^{1/2}\left(\frac{1-z}{2}\right)^{1/2}} d\Omega_{\boldsymbol{x}} d\Omega_{\boldsymbol{y}} \\ &= -\frac{1}{32}(1+z)^{1/2}(1-z)^{1/2} dz d\Omega_{\boldsymbol{x}} d\Omega_{\boldsymbol{y}} \\ &= -\frac{1}{2^5} W(z) dz d\Omega_{\boldsymbol{x}} d\Omega_{\boldsymbol{y}}, \end{aligned} \tag{3.38}$$

where

$$W(z) = (1+z)^{1/2}(1-z)^{1/2} \tag{3.39}$$

is the weight function in the Gauss-Jacobi quadrature. In practice, the variable z is a zero of the Jacobi polynomials. With the transformation (3.37), equation (3.16)

becomes

$$\begin{aligned}\mathcal{P}_K^{\ell_x,\ell_y}(\alpha) &= N_K^{\ell_x\ell_y}\left(\frac{1+z}{2}\right)^{\frac{\ell_x}{2}}\left(\frac{1-z}{2}\right)^{\frac{\ell_y}{2}}P_n^{\ell_x+\frac{1}{2},\ell_y+\frac{1}{2}}(z) \\ &= \frac{1}{2^{\frac{(\ell_x+\ell_y)}{2}}}N_K^{\ell_x,\ell_y}(1+z)^{\frac{\ell_x}{2}}(1-z)^{\frac{\ell_y}{2}}P_n^{\ell_x+\frac{1}{2},\ell_y+\frac{1}{2}}(z)\end{aligned} \tag{3.40}$$

In this equation shows that $\mathcal{P}_K^{\ell_x,\ell_y}(\alpha)$ vanishes at $z = \pm 1$ and peaks at $z = 0$. Inserting equations (3.38) and (3.40) into equation (3.36), one obtains

$$\begin{aligned}V^{J(i)}_{\gamma' K',\gamma K}(\rho) &= \frac{1}{2^\theta}\delta_{\gamma\gamma'}\delta_{KK'}N_K^{\ell_x,\ell_y}N_{K'}^{\ell'_{xi},\ell'_y}\int_{-1}^{1}(1+z)^\delta(1-z)^\beta \\ &\times V\left[\rho\left(\frac{1+z}{2}\right)^{1/2}\right]P_n^{\ell_x+\frac{1}{2},\ell_y+\frac{1}{2}}(z)P_{n'}^{\ell'_x+\frac{1}{2},\ell'_y+\frac{1}{2}}(z)dz,\end{aligned} \tag{3.41}$$

where

$$\begin{aligned}\theta &= \frac{(6+\ell_x+\ell_y+\ell'_x+\ell'_y)}{2} \\ \delta &= \frac{(\ell_x+\ell'_x+1)}{2} \\ \beta &= \frac{(\ell_y+\ell'_y+1)}{2}.\end{aligned} \tag{3.42}$$

Despite the oscillatory behavior of Jacobi polynomials, which increases with n, the coupling matrix elements (3.41) will quickly converge due to the short-range nature of the potential $V(x)$, since in our case this potential contains only the nuclear part. One can easily notice that for higher values of orbital angular momenta ℓ_x and ℓ_y, the coupling matrix elements (3.41) rapidly decrease, due to the factor 2^θ. Therefore, higher partial-waves are not expected to have a meaningful effect on the ground-state structure of the system. It follows that $\ell_x = \ell_y = 0$, accounts for the lagest

contribution to the coupling matrix elements.

In order to solve the coupled differential equations (3.29), one needs to also evaluate the coupling matrix elements $V^{J(j)}_{\gamma' K',\gamma K}(\rho)$ and $V^{J(k)}_{\gamma' K',\gamma K}(\rho)$. To this end, we need to find the appropriate HH expansion basis since the expansion basis in equation (3.19) is no longer valid due to different Jacobi coordinates. However, one does not need to start all over again in building new expansion bases for each set of Jacobi coordinates. The basis transformation between different sets of Jacobi coordinates is done as follows [115]

$$\mathscr{Y}^{l_{x_a},l_{y_a}}_{KLM_L}(\Omega_a) = \sum_{l_{x_i} l_{l_{y_i}}} \langle l_{x_i}, l_{y_i} | l_{x_a}, l_{y_a} \rangle \mathscr{Y}^{l_{x_i},l_{y_i}}_{KLM_L}(\Omega_i), \tag{3.43}$$

where $\langle l_{x_i}, l_{y_i} | l_{x_a}, l_{y_a} \rangle$ are Raynal-Revai coefficients [115], with $a \equiv j, k$. The set of coupled equations 3.29, needs to be transformed into an eigenvalue problem for numerical treatment. To this end, we expand the radial wave function $F^J_{\gamma K}(\rho)$ as follows

$$F^J_{\gamma K}(\rho) = \sum_{n=0}^{N} a^J_{\gamma K} R_n(\rho), \tag{3.44}$$

where the basis functions $R_n(\rho)$ are given by

$$R_n(\rho) = \rho^{5/2} \rho_0^{-3} \left[\frac{n!}{(n+5)!} \right]^{1/2} L^5_n(z) e^{-z/2}, \tag{3.45}$$

with $z = \rho/\rho_0 (\rho$ being the scaling radius) and $L^\alpha_n(z)$ is the associated Laguerre polynomial. In equation (3.44), N is the maximum number of basis points that are

needed to guarantee the convergence of the numerical calculations.

3.5 Boundary conditions

In order to solve the coupled differential equations (3.29), one needs to determine the boundary conditions imposed in the radial wave function $F^J_{\gamma K}(\rho)$ at the origin and in the asymptotic region ($\rho \to \infty$). One of the key features of the HHM is that the asymptotic behavior of a three-body system in the hyperadius is similar to that of a two-body system, such that for a bound-state the coupled differential equations are solved subject to the following boundary conditions

$$F^J_{\gamma K}(\rho) \overset{\rho\to 0}{\to} \rho^{\mathscr{L}+1}, \quad F^J_{\gamma K}(\rho) \overset{\rho\to\infty}{\to} \exp(-\kappa\rho), \tag{3.46}$$

where $\kappa = \sqrt{2m_N|\varepsilon_{3b}|}$, is the ground-state wave number.
In the next chapter, we discuss the numerical results obtained for the ^{22}C three-body halo system.

Chapter 4

Results and Discussion

In this chapter, we present and discuss the various results of our numerical calculations. We analyse in detail the relevance of nn and three-body interactions on the ground-state properties of the ^{22}C neutron-halo nucleus. To this end, we study the ground-state binding energy as a function of the strength and ranges of these interactions. The chapter starts with a brief description of the parameters that are involved in the numerical calculations.

4.1 Brief description of the ^{22}C system

The first observation of a bound ^{22}C can be traced back in 1986 [121], and it is modeled as $^{22}\mathrm{C} \rightarrow {}^{20}\mathrm{C} + n + n$. Although earlier measurement reported the $^{21}\mathrm{C} \rightarrow {}^{20}\mathrm{C} + n$ system to be bound [122], a latter measurement found that this system is in fact unbound [123]. As such, the ^{22}C is regarded as a borromean system, where none of the sub-systems is bound. Due to a large matter radius extracted from the measured reaction cross section ($5.4 \pm 0.9\,\mathrm{fm}$) [6], this system is known to be a two-body neutron-halo system [6]. In other words, the ^{22}C is formed by a core nucleus ^{20}C to which two neutrons are weakly-bound. The $I^{\pi} = 0^{+}$ ground-state of the core nucleus predominantly consists of a $(0d_{\frac{5}{2}})^6$ configuration [16]. To support the halo

nature of this system, the two-body subsystems must be either very weakly bound or low-lying resonances, or virtual states must be present, in order to support a halo state [2]. A resonance in the $d_{3/2^+}$ state of the ^{21}C has been suggested in [124]. In the ground-state of the ^{22}C system is $(s_{1/2})^2$ configuration which is predominantly dominated, while other components add rather small admixtures [125, 129]. The ground state of this system consists almost entirely of configurations with total spin of halo neutrons $[s_1 s_2]S = 0$ (with weight more then 98%), which emphasizes the halo structure of this nucleus, and is identified by $J^\pi = 0^+$ [16, 125]. This make-up simplifies the couplings of the angular momenta in Chapter 3.

4.1.1 $n - {}^{20}$C and nn interactions

As for any three-body system, the ground-state properties of the ^{22}C are determined by intercluster (two-body) potentials. The selection of these potentials is complicated by the lack of experimental information on the neutron-^{22}C subsystem, given the fact that a bound-state of ^{21}C does not exist. In this case, we resort to a partial-wave dependent (ℓ-dependent) potential $[V_{n-core}(x)]$ for the $n - {}^{20}$C subsystem. For the $V_{core-n}(x)$, we consider the usual Woods-Saxon potential, with both central and spin-orbit coupling terms, given by equation (2.30). The different parameters of this interaction, taken from Ref. [4], are summarized in Table 4.1. The depth $V_0^{\ell=2} = -47.8\,\text{MeV}$ was selected to produce a neutron separation energy of about 2.93 MeV in the $1d_{\frac{5}{2}^+}$ state of the ^{21}C system. With the same value produces a $3/2^+$ resonance, with energy $\varepsilon_r = 0.83\,\text{MeV}$ as one observes in Fig.4.1. The same depth $V_0^{\ell=0} = -47.8\,\text{MeV}$ was found too strong and produced a bound $2s_{\frac{1}{2}^+}$ state. It was then reduced to $V_0^{\ell=0} = -29.8\,\text{MeV}$ in order to ensure that the $2s_{\frac{1}{2}^+}$ state is unbound. The same depth $V_0^{\ell=0} = -29.8\,\text{MeV}$ was used in other partial waves non-S-wave

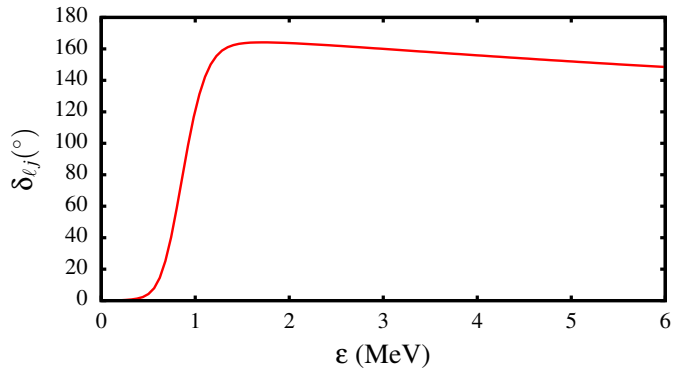

Figure 4.1: Resonance structure of the ^{21}C system in the $1d_{\frac{5}{2}^+}$ state

partial waves other than d-waves.

Table 4.1: Parameters of the core-neutron Woods-Saxon potential, where V_0, $V_{\rm so}$ are the depths of the central and spin-orbit coupling term, and R_i, and a_i $[i \equiv (0, {\rm so})]$, the corresponding absolute radii diffuseness. These parameters were taken from Ref. [4].

ℓ	V_0	R_0	a_0	$V_{\rm SO}$	$R_{\rm SO}$	$a_{\rm SO}$
0	-29.8	3.393	0.65	35	3.393	0.65
2	-47.8	3.393	0.65	35	3.393	0.65

For the nucleon-nucleon (nn) potential, we used a simple Gaussian potential [114], given by

$$V_{nn}(x) = v_0 e^{-(x/x_0)^2}, \tag{4.1}$$

where we tuned the parameters (v_0, x_0) to reproduce the well-known nn scattering length $a_s = -15\,{\rm fm}$. We found that this scattering length is obtained with $(v_0, x_0) = (-31.0\,{\rm MeV}, 1.8\,{\rm fm})$, which are the same pameters in Ref. [114], also adopted in

other works, such as Ref. [130]. With this simple potential, setting $v_0 = 0$, implies that $V_{nn} = 0$. Other choices of the nn potential are available in the literature, such as the Gogny-Pires-Tourreil potential [105], which is one of the commonly used in the three-body calculations. We motivate the choice of this simple interaction by the fact that it contains few parameters, which is convenient for the present study, which involves varying both v_0 and x_0.

4.1.2 Three-body interactions

For the three-body forces, we used two different interactions. The one that is given by the following simple power form

$$V_{3b}(\rho) = \frac{v_{3b}}{1 + \left(\rho/\rho_0\right)^a}, \tag{4.2}$$

where $\rho_0 = 5\,\text{fm}$ defines the range of the potential, $a = 3\,\text{fm}$, and another one of the following Gaussian shape

$$V_{3b}(\rho) = v_{3b} e^{-(\rho/\rho_0)^2}, \tag{4.3}$$

where $\rho_0 = 6\,\text{fm}$. In the discussion of the results, we will denote the interaction (4.2) by P1, and the interaction (4.3), by P2. Both interactions have been used in different studies such as in Refs. [72, 126, 127].

4.2 Details of numerical calculations

In order to numerically solve the coupled differential equations (3.29), various numerical parameters are needed. The coupling matrix elements were numerically evaluated by means of the Gauss-Jacobi quadrature. The number of mesh points used in this calculation was $N_J = 100$. The number of basis points used in the expansion of the radial wave function of the Laguerre basis [equation (3.45)], was $N_L = 80$. The parameter ρ_0 in equation (3.45) was set to $\rho_0 = 0.2\,\text{fm}$. The coupled differential equations were integrated out to $\rho_{\max} = 100\,\text{fm}$, and the interval $[0 : \rho_{\max}]$ was sliced into 1000 equally spaced mesh points. The orbital angular momenta ℓ_x and ℓ_y were truncated to a maximum value of $(\ell_x, \ell_y)_{\max} = 3$, and the hyperangular momentum K was truncated by $K_{\max} = 40$. These numerical parameters were selected in accordance with the convergence requirement, in particular for a large range of the nn potential, where the wave function was observed to exhibit a long-range behavior. The numerical calculations were performed using the computer code FaCe [42].

4.3 Brief analysis of the expansion basis

In Fig. 4.2, we plot the basis expansion $R_n(\rho)$ of the expansion (3.45), as a function of the hyperadius ρ, for various values of the positive integer n. One observes in that figure that for lower values of n ($n = 2$), the function $R_n(\rho)$ repidly converges to zero for large $\rho \geq 20\,\text{fm}$. For larger values of n, the function $R_n(\rho)$ becomes oscillatory. We also analyzed the behavior of the hyperspherical basis functions $\mathcal{P}_K^{\ell_x,\ell_x}(\alpha)$, given by equation (3.16), which are shown in Fig.4.3, as function of z. The variable z and weight function were determined by the Gauss-Jacobi quadrature. In this figure, the label $\gamma \equiv (n, \ell_x, \ell_y, K)$, standing for some of the various quantum numbers that

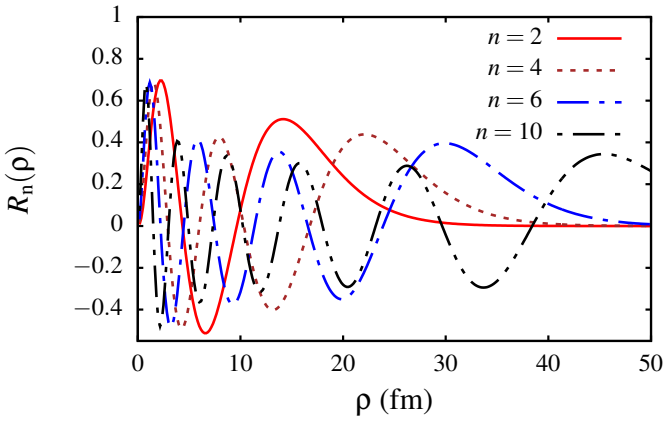

Figure 4.2: Plot of the radial basis function [Eq.(3.45)], for different values of n.

describe the three-body state. As expected, according to equation (3.40), one sees in that figure that the basis function is zero for $z = +1$, and $z = -1$. It becomes highly oscillatory and n increases, which reflects the oscillatory nature of the Jacobi polynomials of higher degrees (higher values of n).

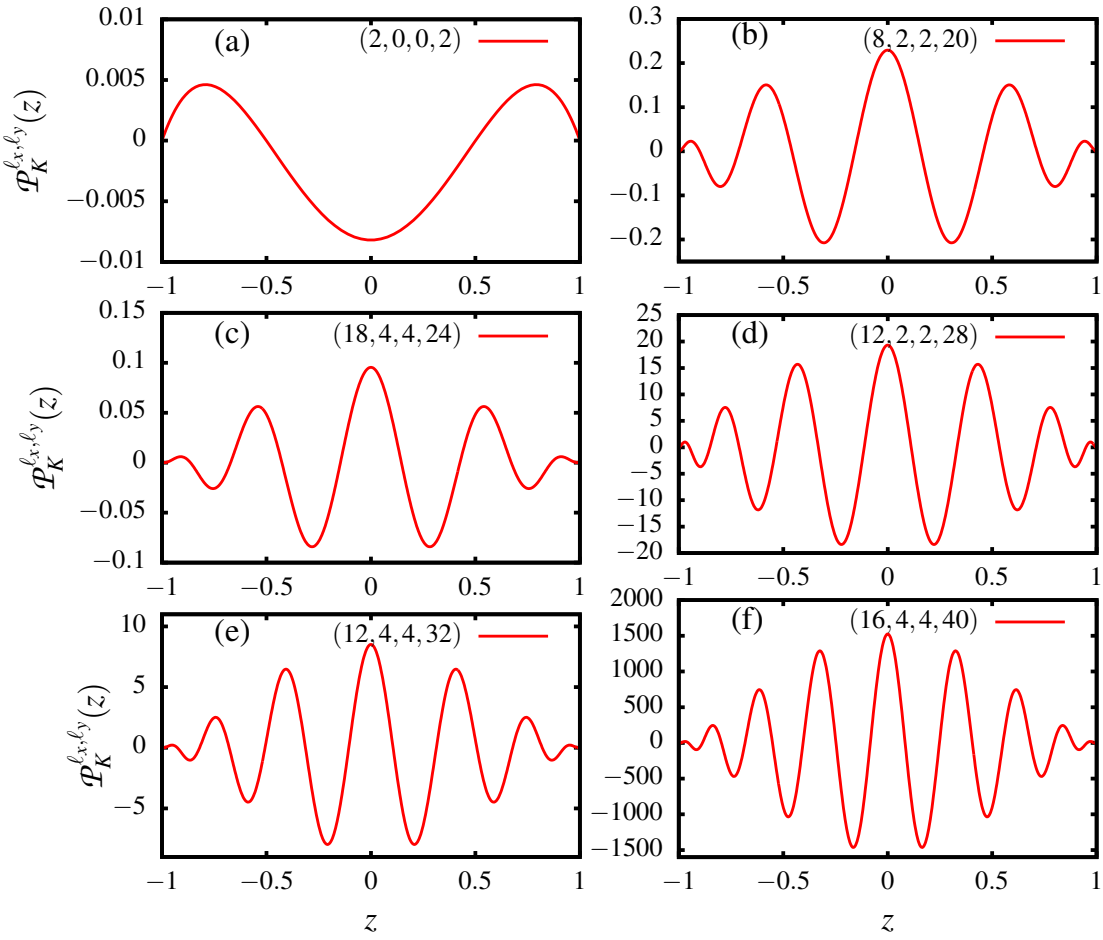

Figure 4.3: Plot of the hyperspherical basis function $\mathcal{P}_K^{\ell_x,\ell_y}(z)$, as function of z. The label $\gamma \equiv (n, \ell_x, \ell_y, K)$ in each panel represents some of the quantum numbers used to describe the three-body state.

4.4 Convergence of the ground-state binding energy as function of $K_{\max}$

We start this section by analyzing the convergence of the three-body ground-state binding energy ε_{3b}. Three different cases using the three-body interaction P1: (i) by

varying the depth v_{3b}, (ii) by removing the nn interaction ($v_0 = 0\,\text{MeV}$), and (iii) by removing the three-body interaction ($v_{3b} = 0\,\text{MeV}$). By so doing, we intend to check the stability of the various calculations. Although the convergence was checked

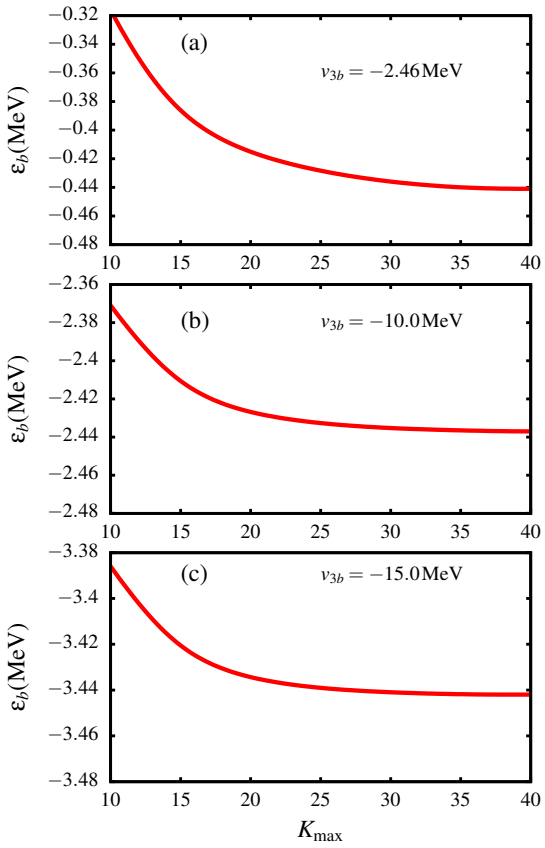

Figure 4.4: Convergence of the three-body ground-state binding energy ε_{3b} as a function of the hypermomentum K_{max}, for three different strengths ($v_{3b} = -2.46\,\text{MeV}, -10\,\text{MeV}, -15\,\text{MeV}$) of the potential P1 [Eq. (4.2)]. The results are obtained with $v_0 = -31.0\,\text{MeV}$, where v_0 is the depth of the nn interaction [Eq. (4.1)].

against other numerical integration parameters, such as ℓ_x, and ℓ_y, we only discuss the convergence of ε_{3b} as a function of the maximum hypermomentum K_{max}. Fig.4.4, displays the convergence of ε_{3b} for three different values ($-2.46\,\text{MeV}$, $-10\,\text{MeV}$ and

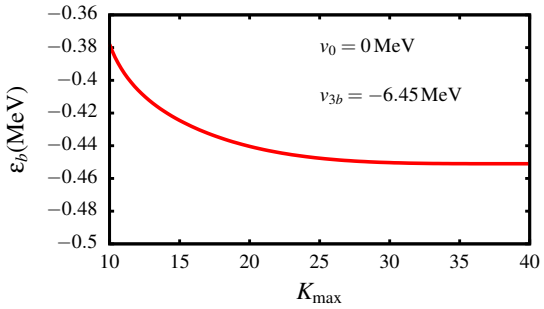

Figure 4.5: Convergence of the three-body ground-state binding energy ε_{3b} as a function of the hypermomentum $K_{\max}$. The depth of the potential P1 is set to $v_{3b} = -6.45$ MeV, in the absence of the nn interaction ($v_0 = 0$).

-15 MeV) of the strength (depth) v_{3b} of the three-body interaction P1. The values -10 MeV and -15 MeV were arbitrary selected, whereas the value -2.46 MeV was adjusted to reproduce $\varepsilon_{3b} = -0.44$ MeV, which is close to one of the two neutrons separation energies assigned to the ^{22}C system in Ref. [29]. The nn interaction is included with $v_0 = -31.0$ MeV, and $x_0 = 1.8$ MeV. Inspecting Fig.4.4, it resorts that the convergence of the binding energy is achieved for all three values of v_{3b}, for $K_{\max} \geq 20$. This implies that the depth of the three-body interaction does not affect the number of partial-waves that are needed to guarantee the convergence of the ground-state binding energy. Another noticeable aspect in Fig.4.4, is that the binding energy increases with the depth of the three-body interaction [see panels (b) and (c) of that figure], which indicates that the system becomes more compact as the three-body interaction becomes more attractive. The convergence of ε_{3b} in the absence of the nn interaction ($v_0 = 0$ MeV, which implies that there are no nn correlations, at least as long as the nn correlations are all removed when $V_{nn} = 0$ MeV), is displayed in Fig.4.5. One also observes that the convergence is achieved for $K_{\max} \geq 20$. To obtain the same ground-state binding energy $\varepsilon_{3b} = -0.44$ MeV, we adjusted the depth of the three-body interaction to $v_{3b} = -6.45$ MeV. The convergence of ε_{3b}

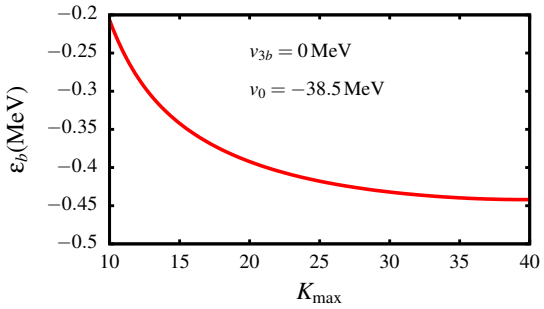

Figure 4.6: Convergence of the three-body ground-state binding energy ε_{3b} as a function of the hypermomentum $K_{\max}$, in the absence of the three-body interaction ($v_{3b} = 0$). The depth of the nn interaction is set to $v_0 = -38.5\,\text{MeV}$.

when there is no three-body interaction ($v_{3b} = 0\,\text{MeV}$) is displayed in Fig.4.6. One notices that the convergence is also achieved. Also, to obtain the same binding energy $\varepsilon_{3b} = -0.44\,\text{MeV}$, the depth of the nn interaction was increased to $v_0 = -38.5\,\text{MeV}$. In the light of the results in Figs.4.4-4.6, one can draw the following conclusion. In the absence of the three-body interaction, the three-body system is bound by a more attractive nn interaction. Likewise, in the absence of the nn interaction, the system is bound by a more attractive three-body interaction. This amounts to saying that the depths of these interactions play a complementary role in the three-body system, at least as far as the present system is concerned.

4.5 Ground-state binding energy versus the strength v_{3b}

In order to better display the relevance of the strength of the three-body interaction on the ground-state binding energy, we show in Table 4.2, the binding energies for the three selected values of the depth v_{3b} of the three-body interactions P1 and

Table 4.2: Three-body ground state binding energies ε_{3b} (in MeV), for different values of the depth of the three-body interaction given by Eqs.(4.2) and Eq.(4.3). P1 represents the interaction (4.2), and P2 the interaction (4.3). Setting $v_0 = 0$ means that the nn interaction is removed, meaning that there are no nn correlations.

	v_{3b}	-2.46MeV	-10 MeV	-15 MeV
P1	$v_0 = -31$ MeV	-0.441	-2.437	-3.442
	$v_0 = 0$ MeV	–	-1.186	-1.972
P2	$v_0 = -31$ MeV	-0.373	-2.274	-3.264
	$v_0 = 0$ MeV	–	-0.952	-1.723

P2, when the nn is included ($v_0 = -31.0$ MeV), and excluded ($v_0 = 0$ MeV). For example, it is seen in that table, that for $v_{3b} = 10$ MeV, $\varepsilon_{3b} = -2.437$ MeV, whereas for $v_{3b} = 15$ MeV, $\varepsilon_{3b} = -3.442$ MeV, for the potential P1. When the nn interaction is removed we found that the system is no longer bound for $v_{3b} = -2.46$ MeV, but is bound for $v_{3b} = -10$ MeV, -15 MeV. This can further proves that for the considered system, a shallower three-body interaction cannot produce a three-body bound system in the absence of the nn interaction. To verify whether this observation is dependent on the shape of three-body interaction, we also show Table 4.2, the results obtained with the interaction P2. Although the numbers are slightly lower compared to the interaction P1, the same trend is maintained. The dash mark ($-$) in Table 4.2, serves to indicate that there is no bound-state for the particular parameters. We extended the radial integration up to $\rho_{max} = 1000$ fm, but still a bound-state could not be found for $v_{3b} = -2.46$ MeV and $v_0 = 0$ MeV.

4.6 Ground-state binding energy versus the strength v_0

In Table 4.3, we also analyze the dependence of the three-body binding energy on the strength of the nn interaction. To this end, we also selected three values $v_0 = -31\,\text{MeV}$, $-38.5\,\text{MeV}$ and $-60\,\text{MeV}$. The value $-60\,\text{MeV}$, was arbitrarily selected whereas the value $-38.5\,\text{MeV}$ was adjusted to obtain the binding energy $\varepsilon_{3b} = -0.441\,\text{MeV}$ in the absence of the three-body interaction. An observation of that table shows that the binding energy increases as well with the strength of the nn interaction. One further notes that in the absence of the three-body interaction, the binding energy decreases significantly ($\varepsilon_{3b} = -0.067\,\text{MeV}$) for $v_0 = -31\,\text{MeV}$, suggesting that for $v_0 \ll -31\,\text{MeV}$, a bound state might not be expected in the absence of the three-body interaction.

Table 4.3: Three-body ground state binding energies ε_{3b} (in MeV), for different values of the v_0 depth of the nn interaction given by Eq.(4.1). We only consider the three-body interaction P1. Setting $v_{3b} = 0\,\text{MeV}$ means that the three-body interaction is removed.

v_0(MeV)	-31MeV	-38.5 MeV	-60 MeV
$v_{3b} = -2.46\,\text{MeV}$	-0.441	-0.962	-1.845
$v_{3b} = 0$ MeV	-0.067	-0.441	-1.706

4.7 Ground-state binding energy versus the range ρ_0 of the three-body interaction

So far, our analysis has focused on the binding energy as a function of the strengths of the nn and three-body interactions. Another crucial parameter to consider is the range of these interactions. For instance, apart from the ^{22}C and ^{20}C matter radii, the range of the three-body interaction may as well reflect the fact that the two halo neutrons are located outside the ^{20}C core nucleus. If for example the range ρ_0 is such that $\rho_0 \ll R_c$ [where R_c, is the root-mean-square (rms) matter radius of the ^{20}C core nucleus], one may not expect a bound ^{22}C system, mainly because such range would be too short to reach the peripheral neutrons. Also, in a three-body system, the two halo neutrons are known to be far from each other, making the range of the nn interaction an important parameter. The results so far presented were obtained with the range of the three-body interaction set to $\rho_0 = 5\,\text{fm}$ for the interaction P1 and $\rho_0 = 6\,\text{fm}$ for the interaction P2, which is well above $R_c = 2.913\,\text{fm}$ and $R_m = 3.503\,\text{fm}$ (where R_m is the rms matter radius of the ^{22}C system), quoted from [6]. Before we discuss the results, let us first check the behavior of the potential $V_{3b}(\rho)$ for different values of the range ρ_0. In panel (a) of Fig.4.7, this potential is plotted as a function of the hyper-radius ρ where the range given in terms of R_c, considering only the interaction P1. The figure shows that for $\rho_0 = \frac{1}{4}R_c$, the potential vanishes at $\rho \geq 2\,\text{fm}$, and its tail extends to $15\,\text{fm}$ for $\rho_0 = \frac{5}{2}R_c$. In other words, for $\rho_0 = \frac{1}{4}R_c$, the potential vanishes for $\rho \geq R_c$, in which case it may be assimilated to a zero-range interaction. The binding energy as well as the rms matter radii corresponding to different values of ρ_0 up to $\rho_0 = \frac{5}{2}R_c$, are presented in Table 4.4, considering only the interaction P1, with $v_{3b} = -2.46\,\text{MeV}$.We show the

results obtained when the nn interaction is included ($v_0 = -31\,\text{MeV}$) and when it is excluded ($v_0 = 0\,\text{MeV}$). The rms matter radius was calculated as follows [86]

$$\begin{aligned} R_m &= \sqrt{\frac{A_c}{A}R_c^2 + \frac{\langle\rho^2\rangle}{A}}, \\ &= \sqrt{\frac{1}{A_c+2}\Big(R_c^2 + \langle\rho^2\rangle\Big)} \end{aligned} \tag{4.4}$$

where $A = 22$ and $A_c = 20$, are the atomic mass numbers, and $\langle\rho^2\rangle$ the mean-squared hyper-radius, obtained from the radial wave function $F_\beta^J(\rho)$ as follows

$$\langle\rho^2\rangle = \sum_\beta \int_0^\infty d\rho\rho^2 \big|F_\beta^J(\rho)\big|^2. \tag{4.5}$$

Looking at Table 4.4, one sees that the binding energy is a continuous function of the range ρ_0, meaning that it increases with the range of the potential. In other words, as ρ_0 increases, reaching even beyond the peripheral neutrons, the system becomes more compact. For $\rho_0 = \frac{1}{4}R_c$ and $\rho_0 = \frac{1}{2}R_c$, the system is very weakly-bound, with $\varepsilon_{3b} = -0.069\,\text{MeV}$ and $= -0.077\,\text{MeV}$, respectively. As seen in Fig.4.7, for these two values, the potential vanishes rapidly beyond $\rho = R_c$. One may then urgue that for $\rho_0 \ll R_c$, the system might not be bound. In this case, the three-body potential being assimulated to a zero-range potential, its depth v_{3b} should be strong enough to provide a bound-state, alluding to the three-body Thomas effect [128]. When the nn interaction is removed, the system becomes only bound for $\rho_0 \geq 2R_c$. In the light of this result, one may argue that in the absence of nn interaction, the two independent neutrons are located further away from the core nucleus, such that a long-range three-body interaction is required in order to sustain a bound-state. This is consistent with the fact that when the nn interaction is removed, the binding

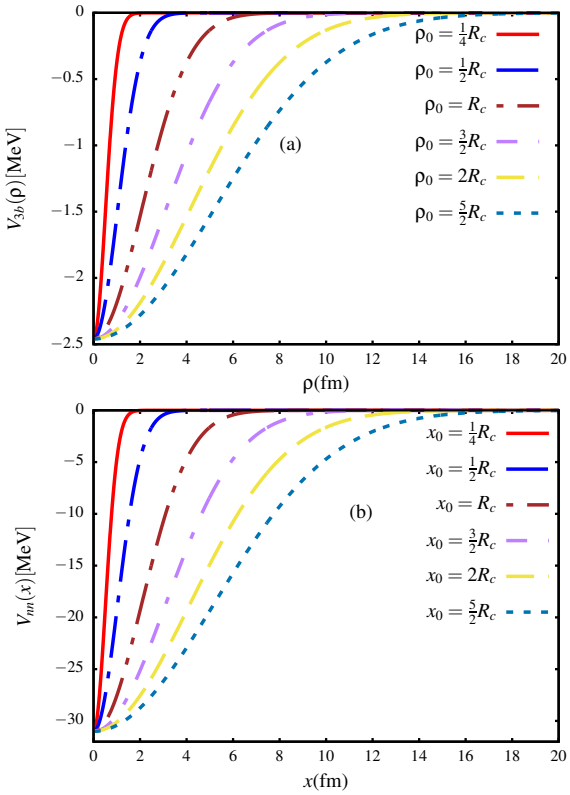

Figure 4.7: Plot of the three-body potential $V_{3b}(\rho)$ given by Eq. (4.2) as function of the hyperadius ρ for different values of the range ρ_0 [panel (a)] and of the nn interaction $V_{nn}(x)$ given by Eq.(4.1) as function of nn coordinate x, for different values of the range x_0.

energy decreases (see Tables 4.2 and 4.4). Since the binding energy increases with the range ρ_0, this implies that that the rms matter radius R_m decreases and this what is observed in Table 4.4. This is also well depicted in Fig.4.8, where the binding energy and rms matter radius are plotted as functions of the range ρ_0. With $\rho_0 = 5.0\,\text{fm}$, we obtained the same value $R_m = 3.503\,\text{fm}$ as in Ref. [6].

Table 4.4: Dependence of the three-body ground-state binding energy ε_{3b} and the ^{22}C root mean-square matter radius R_m, for $v_{3b} = -4\,\text{MeV}$, $v_0 = -31.0\,\text{MeV}$, and $v_0 = 0.0\,\text{MeV}$.

	ρ_0	$\frac{1}{4}R_c$	$\frac{1}{2}R_c$	R_c	$\frac{3}{2}R_c$	$2R_c$	$\frac{5}{2}R_c$
$v_0 = -31$	ε_{3b} (MeV)	-0.069	-0.077	-0.145	-0.327	-0.609	-0.913
	R_m (fm)	4.548	4.482	4.110	3.738	3.551	3.476
$v_0 = 0$	ε_{3b} (MeV)	–	–	–	–	-0.050	-0.244
	R_m (fm)	–	–	–	–	4.910	3.823

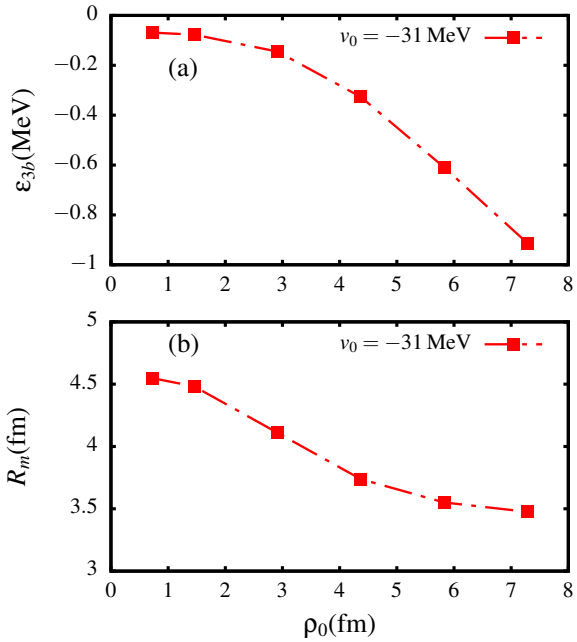

Figure 4.8: Ground-state binding energy ε_{3b} [panel (a)], and rms matter radius [panel (b)], as functions of the range of the three-body interaction (4.2).

4.8 Ground-state binding energy versus the range x_0 of the nn interaction

Let us now turn to the effect of the range x_0 of the nn interaction. The plot of this interaction as a function of the nn coordinate x is shown in panel (b) of Fig.4.7, for different values of the range x_0 also given in terms of R_c. We observe in that figure that for $x_0 = \frac{1}{4}R_c$, this interaction is confined within $x = 2\,\text{fm}$, which is less than R_c. One notes that the interaction extends beyond $x = 14\,\text{fm}$ for $x_0 = \frac{5}{2}R_c$, which is about 5 times the size of the core nucleus and about 4 times the size of the three-body system. The various binding energies and rms matter radii obtained for various values of the range x_0 are shown in Table 4.5. They were obtained when the three-body interaction is included and excluded in the calculations. We found that the system is not bound for $x_0 = \frac{1}{4}R_c$, and extremely weakly-bound ($\varepsilon_{3b} \simeq 3\,\text{eV}$) for $x_0 = \frac{1}{2}R_c$. It is also observed that the binding energy increases with the range x_0 as it is with ρ_0 in Table 4.4. In the absence of the three-body interaction ($v_{3b} = 0$), the table shows that the system is only bound for $x_0 \geq R_c$. The results are also plotted as function of x_0 in Fig.4.9, for a better display.

For completeness, we analyze the radial ground-state wave functions, $F^J_\beta(\rho)$, considering only the more dominant s-wave component, i.e., $\beta \equiv (0,0,0,0,0)$. This component is shown in Fig.4.10, for values of the ranges ρ_0 [panel (a)] and x_0 [panel (b)]. In both panels of that figure, we obtain the expected behavior of the bound-state wave function for a weakly-bound system, where a smaller binding energy, corresponds to a longer tail of the wave function.

Table 4.5: Dependence of the three-body ground-state binding energy ε_{3b} and rms matter radius R_m on the range x_0 of the nn interaction. Cases where the three-body interaction is included ($v_{3b} = -2.46\,\text{MeV}$) and excluded ($v_{3b} = 0.0\,\text{MeV}$) are considered.

	x_0	$\frac{1}{4}R_c$	$\frac{1}{2}R_c$	R_c	$\frac{3}{2}R_c$	$2R_c$	$\frac{5}{2}R_c$
$v_{3b} = -2.46$MeV	ε_{3b} (MeV)	–	-0.000	-0.296	-1.437	-1.919	-2.044
	R_m (fm)	–	5.615	3.817	3.458	3.321	3.314
$v_{3b} = 0$	ε_{3b} (MeV)	–	–	-1.778	-1.861	-1.900	-2.159
	R_m (fm)	–	–	3.352	3.348	3.330	3.325

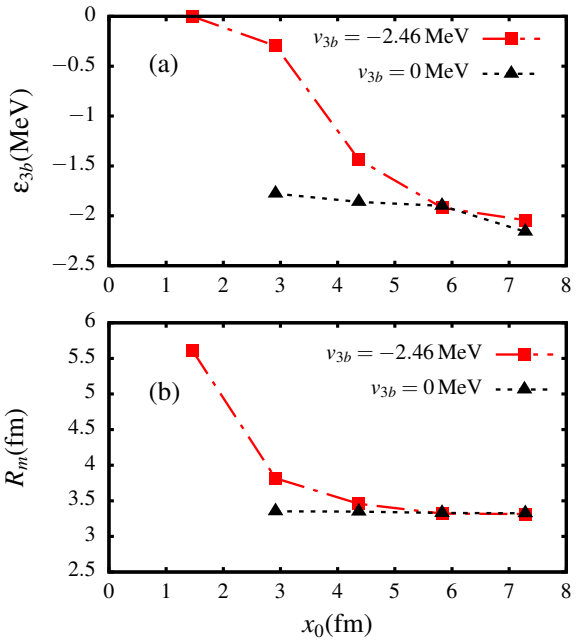

Figure 4.9: Ground-state binding energy ε_{3b} [panel (a)], and root-mean-square matter radius [panel (b)], as functions of the range x_0 of the nn interaction when the three-body interaction is included ($v_{3b} = -2.46\,\text{MeV}$) and excluded ($v_{3b} = 0\,\text{MeV}$)

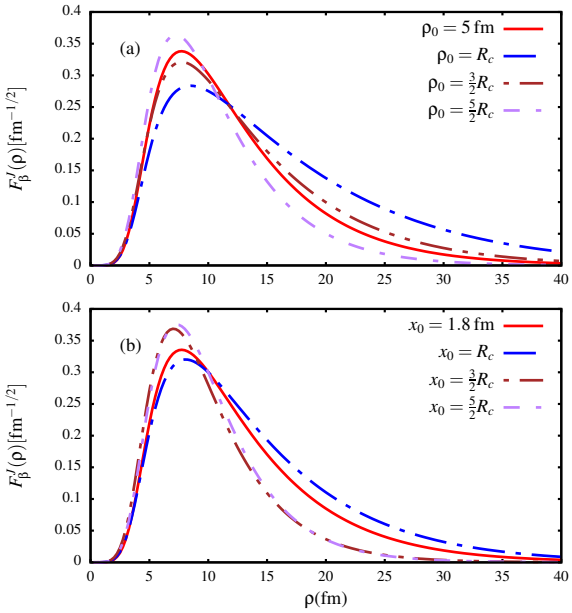

Figure 4.10: Plots of the s-wave component of the ground-state radial wave function for different values of the range ρ_0 of the three-body interaction [panel (a)] and the range x_0 of the nn interaction [panel (b)], and for $v_{3b} = -2.46\,\text{MeV}$ and $v_0 = -31.0\,\text{MeV}$.

4.9 Some ground-state thermodynamic properties

This section is devoted to the study of some of the properties of the ground-state from a thermodynamical point of view. Thermodynamic properties of the ground-state such as mean energy U, entropy S, free energy F, and heat capacity C, of the system can be obtained by using the ground-state binding energy. This requires the knowledge of the partition function z of the system, which is given by [131,132]

$$Z = \sum_{n=0}^{n_{max}} e^{-\mu\varepsilon_n}, \tag{4.6}$$

where ε_n represents the energy levels of the system, $\mu = (k_{\mathrm{B}}T)^{-1}$, with k_{B} being the Boltzmann constant, and T is the temperature at thermodynamic equilibrium. Setting $y = e^{-\mu\varepsilon_n}$ and applying the geometric progression to z, one obtains [133]

$$Z = y + y^3 + y^5 + y^7 = \frac{y}{1-y^2} = \frac{1}{e^{\mu\varepsilon_n} - e^{-\mu\varepsilon_n}}. \tag{4.7}$$

Applying Euler formula

$$e^x - e^{-x} = 2\sinh x, \tag{4.8}$$

equation (4.7) reduces to

$$Z = \frac{1}{2\sinh(\mu\varepsilon_n)}. \tag{4.9}$$

4.9.1 Mean Energy

The mean energy is given in terms of the partition function by

$$\begin{aligned} U &= -\frac{\partial \ln Z}{\partial \beta} = k_{\mathrm{B}} T^2 \frac{\partial \ln Z}{\partial T} \\ &= -\frac{\varepsilon_n}{2} \coth(\beta \varepsilon_n) \end{aligned} \tag{4.10}$$

4.9.2 Free energy

The free energy is given in terms of the partition function by

$$F = -\frac{1}{\beta} \ln Z = -k_{\mathrm{B}} T \ln \left[\frac{1}{2 \sinh(\beta \varepsilon_n)} \right] \tag{4.11}$$

4.9.3 Entropy

The entropy is given in terms of the partition function by

$$\begin{aligned} S &= k_{\mathrm{B}} \ln Z - k_{\mathrm{B}} \mu \frac{\partial \ln Z(\mu)}{\partial \mu} \\ &= k_{\mathrm{B}} \ln Z + \frac{\varepsilon_n}{2T} \coth(\beta \varepsilon_n) \\ &= k_{\mathrm{B}} \ln \left[\frac{1}{2 \sinh(\beta \varepsilon_n)} \right] + \frac{\varepsilon_n}{2T} \coth(\beta \varepsilon_n). \end{aligned} \tag{4.12}$$

4.9.4 Heat capacity

The heat capacity is given in terms of the partition function by

$$\begin{aligned} C &= \frac{\partial U}{\partial T} = -k_{\mathrm{B}}\mu^2 \frac{\partial^2}{\partial \mu^2} \ln Z \\ &= \frac{\varepsilon_n^2}{2k_{\mathrm{B}}T^2} cosech^2(\beta\varepsilon_n). \end{aligned} \tag{4.13}$$

4.9.5 Condition of calculations and results

In the calculations, we converted the three-body ground-state binding energy ε_{3b} from megaelectron volt (MeV) to Kelvin (K) using $1\,\mathrm{MeV} = 1.16 \times 10^{10}\,\mathrm{K}$, and $k_{\mathrm{B}} = 1.38 \times 10^{-23}\,\mathrm{J/K}$. In this case, we obtain $\varepsilon_{3b}/k_{\mathrm{B}}T = 10^{10}\,\mathrm{K} \times \varepsilon_{3b}/T$. With the tempereture T in Kelvin, this ratio is dimensionless. In our numerical calculations, we considered the temperature in gigakelvin (GK), such that $\varepsilon_{3b}/k_{\mathrm{B}}T = 10 \times \varepsilon_{3b}$. In order to test the relevance of the binding energy on the different thermodynamic propoerties, we considered three different binding energies. In Fig.4.11, we show the partition function in terms of the temperature T for three different ground-state binding energies. As one observes in this figure, the temperature increases, the partition function decreases rapidly, in accordance with equation (4.9). The mean free energy is shown in Fig.4.12. We notice that the mean free energy increases with the ground-state binding energy. It is also observed that as the energy increases, the mean free energy appears to become more almost independent of the temperature at low temperature. The free energy is shown Fig.4.13, where we observe that it actually represents the inverse of the mean free energy, where it decreases as the temperature increases.

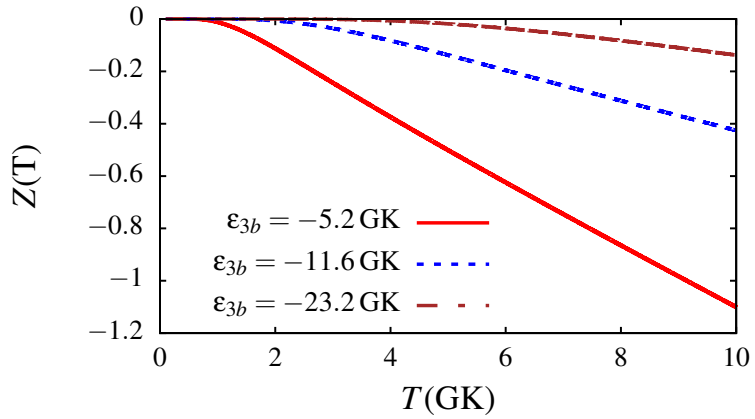

Figure 4.11: Partition function of the ^{22}C system as function of the temperature in (GK) for different ground-state binding energies ε_{3b}.

The entropy is plotted in Fig.4.14, where we observe that it actually tends to infinity at very low temperatures and approaches zero for higher temperature. This figure also shows that the entropy decreases with the energy.

The specific heat capacity is plotted in Fig.4.15. We notice that it is tends to zero at low temperatures and appears to weakly depend on the temperature for higher temperature. One also sees that the heat capacity is weakly dependent on the binding energy for higher temperatures. The results are showing the significance of a low binding energy of the system's thermodynamic properties. It could be interesting to expand on this preliminary study of the thermodynamics properties of weakly-bound halo systems. The study of the uncertainty measures in three-body weakly-bound systems such as Fisher information and the Shanon entropy is a subject of interest.

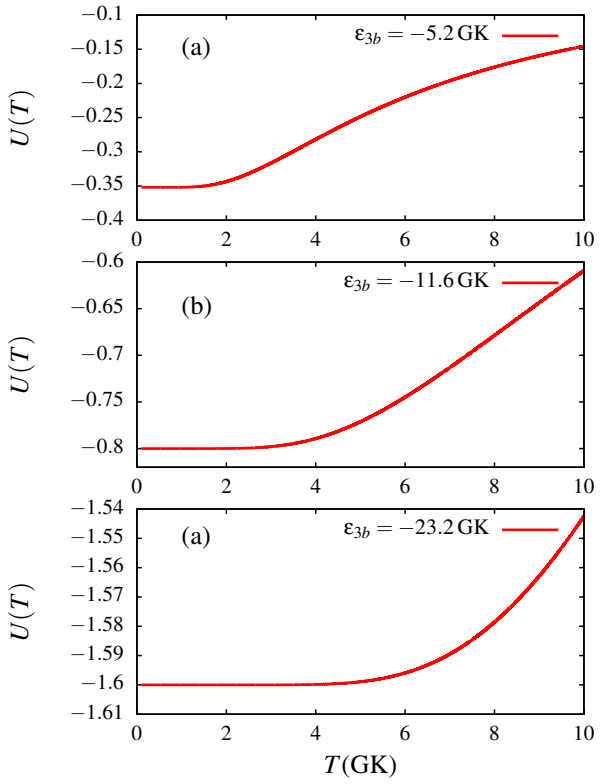

Figure 4.12: Mean energy of the ^{22}C system as function of the temperature in (GK) for different ground-state binding energies ε_{3b}.

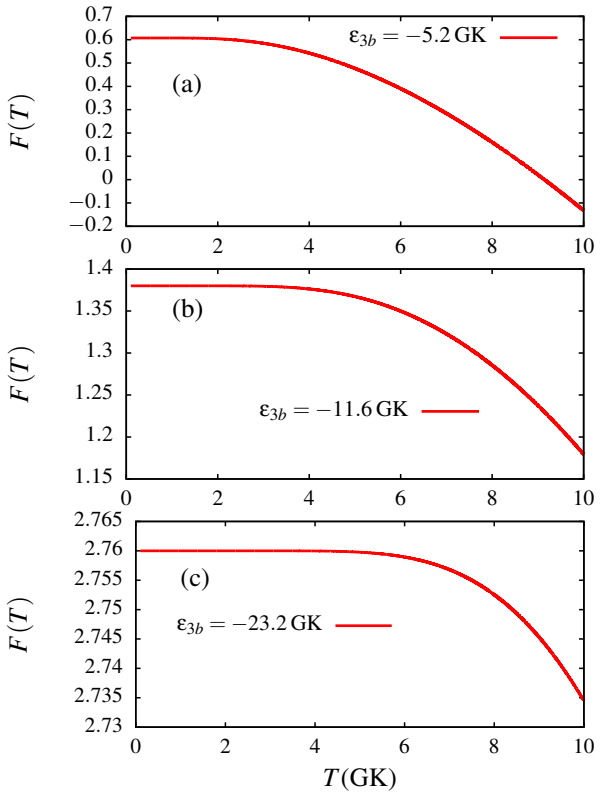

Figure 4.13: Free energy of the ^{22}C system as function of the temperature in (GK) for different ground-state binding energies ε_{3b}.

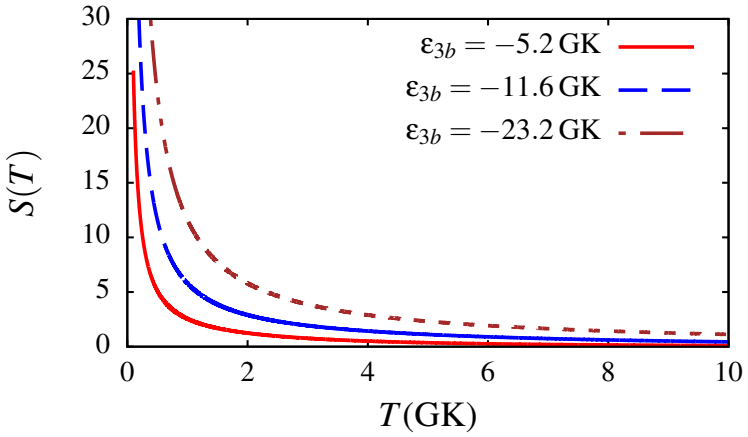

Figure 4.14: Entropy of the ^{22}C system as function of the temperature in (GK) for different ground-state binding energies ε_{3b}.

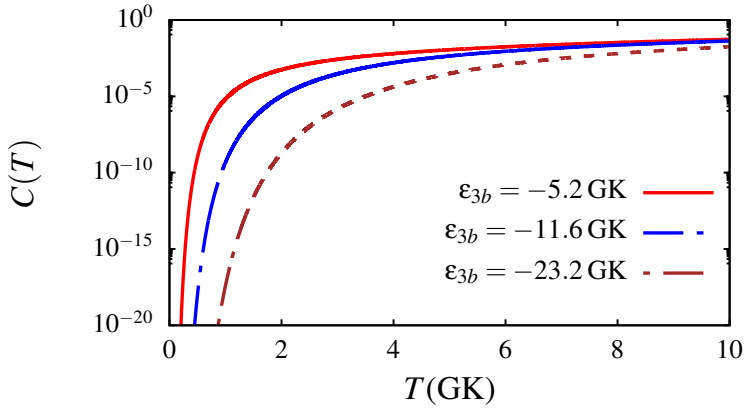

Figure 4.15: Specific heat capacity of the ^{22}C system as a function of the temperature in (GK) for different ground-state binding energies ε_{3b}.

Chapter 5

Conclusion

In this dissertation, we have presented a detailed analysis of the role of the strengths and ranges of the nucleon-nucleon (nn) and three-body interactions on the ground-state properties of a three-body neutron-halo system, considering the ^{22}C system. To this end, we performed several calculations by varying the strengths and ranges of both interactions. We started by outlining the theoretical formulation of a three-body problem, starting with the fundamentals of two-body bound and scattering states. The different steps leading to the transformation of the three-body Schrödinger equation into a one-dimensional set of coupled differential equations are outlined. These equations were numerically solved subject to the appropriate boundary conditions, in order to obtain the three-body ground-state binding energy and wave function. We then investigated how varying the different potential parameter affect the binding energy. Varying the strength of the three-body interaction, it is found that the three-body system remains bound even when the nn interaction is removed, provided the three-body interaction is more attractive (i.e., its strength is increased). Likewise, by varying the strength of the nn interaction it is shown that the three-body system remains bound in the absence of the three-body interaction, provided the nn interaction is more attractive. We then inferred that the strength of the nn and three-body interactions are complementary in a three-body system, at least as

far as the system considered is concerned. We also found the ground-state binding energy to be a continuous function of the strength and range of both interactions, meaning that when these parameters increase, the binding energy increases as well, making the system to be more compact. It could be interesting to perform a similar system on a light borromean system such as ^{6}He. A comparison with the present study would clearify the effect of the core mass and radius on the binding energy of the system. To some extent, it could also elucidate the effect of the core nucleus on nucleon-nucleon correlations in a three-body system.

We also analyzed the ground-state thermodynamic properties of this system. With the knowledge of the partition function which is dependent on the ground-state binding energy, we calculated the mean energy, the free energy, the entropy as well as the heat capacity of the system. The study of the uncertainty measures in three-body weakly-bound systems such as Fisher information and the Shanon entropy is a subject of interest.

Bibliography

[1] I. Tanihata *et al.*, Phys. Rev. Lett. **55**, 2676-2679 (1985)

[2] A.S. Jensen, K. Riisager and D.V Ferodov, Rev. Mod. Phys. **76**, 215 (2004)

[3] Y. Kucuk and J.A. Tostevin, Phys. Rev. **C 89**, 3 (2014)

[4] E.C. Pinilla and P. Descouvemont, Phys. Rev. **C 94**, 2 (2016)

[5] N.B. Shulgina *et al.*, Phys. Rev. **C 97** (2018)

[6] K. Tanaka *et al.*, Phys. Rev. Lett. **104** (2010)

[7] E.C. Pinilla and P. Descouvemont, EPJ Web of Conference **117** (2016)

[8] E.C. Pinilla and P. Descouvemont, J. Phys.:Conf. Ser., **863** (2017)

[9] L. Gaudefroy *et al.*, Phys. Rev. Lett. **109**, 202503 (2012)

[10] Y. Togano *et al.*, Phys. Lett. **B 761**, 412 (2016)

[11] A. Ismail *et al.*, AIP Conference Proceedings **1621** (2014)

[12] F. Hakeem *et al.* , AIP Conference Proceedings **1799** (2017)

© University of South Africa 2023

[13] M.T.Yamashita *et al.*, Phys. Lett. **B 697**, 90 (2011)

[14] M. Alam *et al.*, Proc. DAE Symp. Nucl. Phys. **62** (2017)

[15] T. Frederico *et al.*, Part. Nucl. Phys. **67**, 939 (2012)

[16] W. Horiuchi and Y. Suzuki, Phys. Rev. **C 74**, 3 (2006)

[17] M. Sharma *et al.*, Proceedings of the DAE Symp. on Nucl. Phys. **55** (2010)

[18] L.A. Souza, E. Garrido and T. Frederico, Phys. Rev. **C 94**, 064002 (2016)

[19] S.N Ershov, J.S. Vaagen and M.V. Zhukov, Phyics of Atomic Nuclei **77** (2014)

[20] S.N. Ershov, J.S. Vaagen , and M.V. Zhukov, Phys. Rev. **C 86**, 034331 (2012)

[21] B. Acharya,C. Ji, and D.R. Phillips, Phys. Lett. **B 723**, 196 (2013)

[22] J. Singh *et al.*, *Few-Body Systems* **60** (2019)

[23] X. Sun, J. Zhao and S. Zhou, Phys. Lett. **B 785** (2018)

[24] T. Nagahisa and W. Horiuchi, Phys. Rev. **C 97** (2018)

[25] T. Inakura ,W. Horiuchi ,Y. Suzuki and T. Nakatsukasa, Phys. Rev. **C 89**, 064316 (2014)

[26] Y. Kucuk and J.A. Tostevin *Journal of Physics Conference Series* **381** (2012)

[27] L. Tomio *et al.*, *International Journal of Modern Physics E* **20** (2011)

[28] H.T. Fortune and R. Sherr, Phys. Rev. **C 85**, 027303 (2012)

[29] G. Audi and A.H. Wapstra, Nucl. Phys. **A 729**, 33 (2003)

[30] W. Wang *et al.*, Chin. Phys. **C 41**, 030003 [See also https://www.nndc.bnl.gov/nudat2/] (2017)

[31] K. Ogata *et al.*, Phys. Rev. **C 88**, 024616 (2013)

[32] T. Suzuki *et al.*, Phys. Lett. **B 753**, 199 (2016)

[33] N. Kobayashi *et al.*, Phys. Rev. Lett. **112**, 242501 (2014)

[34] I. Hamamoto, Phys. Rev. **C 95**, 044325 (2017)

[35] X.N. Cao, Q. Liu and J. Y. Guo, Phys. Rev. **C 99**, 014309 (2019)

[36] T. Nakamura *et al.*, Phys. Rev. Lett. **103**, 262501 (2009) .

[37] S. Watanabe *et al.*, Phys. Rev. **C 89**, 044610 (2014)

[38] H. L. Crawford *et al.*, Phys. Rev. Lett. **122**, 052501 (2019)

[39] D.S. Ahn *et al.*, Phys. Rev. Lett. 123, 212501 (2019)

[40] M. Rodriguez-Gallardo *et al.*, Phys. Rev., **C 72** (2005)

[41] de Diego R, Garrido E, Fedorov D V, and Jensen A S, Europhys. Lett. **90**, 52001 (2010)

[42] Thompson I J, Nunes F M, and Danilin B, Comput. Phys. Commun. **161**, 87 (2004)

[43] A.N. Ikot *et al.*, Eur. Phys. J. Plus **134**, 386 (2019)

[44] J. Pliva, J. Mol. Spectrosc. **193**, 193 (1999)

[45] P.G. Hajigeorgiou, J. Mol. Spectrosc. **235**, 111 (2006)

[46] C.A. Singh, O.B. Devi, Int. J. Quantum Chem. **106**, 415 (2006)

[47] A. Durmus, F. Yasuk, J. Chem. Phys. **126**, 074108 (2007)

[48] C. Berkdemir, A. Berkdemir, J. Han, Chem. Phys. Lett. **417**, 326 (2006)

[49] J.F. Ogilvie, *The vibrational and Rotational Spectrometry of Diatomic Molecules* (Academic Press, New York, 1998) p.130

[50] O. Bayrak, I. Boztosun, H. Cifti, Int. J. Quantum Chem. **107**, 540 (2007)

[51] S.H. Dong, *Wave Equation in Higher Dimensions* (Springer, Berlin, 2011)

[52] C.S. Jia *et al.*, Chem. Phys. Lett. **676**, 150 (2017)

[53] K.J. Oyewumi *et al.*, J. Math. Chem. **51**, 976 (2013)

[54] K.R. Purohit, R.H. Parmar, A.K. Rai, Annals of Physics **424**,168335 (2021)

[55] B.J. Falaye *et al.*, Phys. Scr. **89**,115204 (2014)

[56] L.D Faddeev, Sov. Phys. JETP **2** (1961)

[57] S.P Merkuriev, Theor. Math. Phys. **8**, 798 (1971)

[58] S.P Merkuriev, Theor. Math. Phys. **32**, 680 (1977)

[59] S.P Merkuriev, Lett. Math. Phys. **3**, 141 (1979)

[60] S.P Merkuriev, Ann. Phys. **130**, 395 (1980)

[61] S.P Merkuriev *et al.*, Ann. Phys. **99**, 30 (1976)

[62] V.V Kostrykin *et al.*, *Few-Body Systems* **6**, 97 (1989)

[63] A.A Kvitsinsky *et al.*. Sov. Phys. Dokl. **33**, 499 (1988)

[64] M. Fabre de la Ripelle *et al.*, Phys. Rev. **C 38**, 449-466 (1988)

[65] M. Fabre de la Ripelle, Ann. Phys. **147**, 281-320 (1983)

[66] M. Viviani *et al.*, Phys. Rev. **C 71**, 024006 (2005)

[67] S. Leblond *et al.*, Phys. Rev. Lett. **121**, 262502 (2018)

[68] E. Hiyama ,R. Lazauskas ,F.M. Marqués , and J. Carbonell, Phys. Rev. **C 100**, 011603(R) (2019)

[69] Z.H. Yang *et al.*, Phys. Rev. Lett. **126**, 082501 (2021)

[70] N. Keeley *et al.*, Prog. Part. Nucl. Phys. **59**, 579-630 (2007)

[71] J. Casal and J. Gomez-Camacho, Phys. Rev. **C 99** (2019)

[72] J. Casal *et al.*, Phys. Rev. **C 102** (2020)

[73] J. Casal and E. Garrido, Phys. Rev. **C 102** (2020)

[74] B. Mukeru, M.L. Lekala and A.S. Denikin, J. Phys. G: Nucl. Part. Phys. **42** (2015)

[75] J. Singh *et al.*, Phys. Rev. **C 101** (2020)

[76] L. Zhang *et al.*, Phys. Rev. **C 91**, 2 (2015)

[77] L.V. Grigorenko *et al.*, Phys. Rev. **C 80** (2009)

[78] R. Crespo *et al.*, Phys. Rev. **C 83** (2011)

[79] A.M. Moro and R. Crespo, Phys. Rev. **C 85** (2012)

[80] N. Michel *et al.*, Phys. Rev. **C 101**, 3 (2020)

[81] K. Hagino and H. Sagawa, Phys. Rev. **C 75** (2007)

[82] Y. Suzuki, H. Matsumura and B. Abu-Ibrahim, Phys. Rev. **C 70** (2004)

[83] T. Myo *et al.*, Prog. Part. Nucl. Phys. **79** (2014)

[84] T. Myo, R. Ando and K. Kato, Phys. Lett. **B 691** (2010)

[85] P.C. Sood and Y.R. Waghmare, Nucl. Phys. **46**, 181-192 (1963)

[86] M.V. Zhukov *et al.*, Phys. Rep. **231**, 151-199 (1993)

[87] J. Casal, M. Rodriguez-Gallardo and J.M. Arias, Phys. Rev. **C 88** (2013)

[88] Md A. khan and T.K. Das, PRAMANA J. Phys. **57**, 4 701-716 (2001)

[89] J. Bang and C. Gignoux, Nucl. Phys. **A 313**, 119-140 (1979)

[90] B.V. Danilin *et al.*, Nucl. Phys. **A 632**, 383-416 (1998)

[91] J.A. Tostevin and J.S. Al-Khalili, Phys. Rev. **C 59**, 1 (1999)

[92] Y. Satou *et al.*, Phys. Lett. **B 660**, 4, 320-325 (2008)

[93] C.A. Bertulani and H. Sagawa, Nucl. Phys. **A 588**, 3 , 667-692 (1995)

[94] C. Romero-Redondo *et al.*, Phys. Lett. **B 660**, 1-2 (2008)

[95] C. Romero-Redondo *et al.*, Phys. Rev. **C 77** (2008)

[96] P. Voss *et al.*, Phys. Rev. **C 86** (2012)

[97] A. Revel *et al.*, Phys. Rev. Lett. **120** (2018)

[98] D. Cortina-Gil *et al.*, Eur. Phys. J. **A 10**, 49 - (2001)

[99] A. Delfino *et al.*, Phys. Rev. **C 61**, 5 (2000)

[100] C.A Bertulani, H.W. Hammer and U. van Kolck, Nucl. Phys. **A 712**, 37 - 58 (2002)

[101] D. Baye, Phys. Rep. **565**, 1 - 207 (2015)

[102] I.J Thompson, F.M Nunes and B. Danilin, Comput. Phys. Commun. **161**, 87 (2004)

[103] Abramowitz M and Stegun I 1970 *Handbook of Mathematical Functions* (Dover, New York)

[104] I. J. Thompson and F. M. Nunes, *Nuclear Reactions for Astrophysics* (Cambridge University Press, New York, 2009)

[105] D. Gogny, P. Pires and R. de Tourreil, Phys. Lett. **B32**, 591 (1970)

[106] A.B. Volkov, Nucl. Phys. **74**, 33-58 (1964)

[107] R.A Malfliet and J.A Tjon, Nucl. Phys. **A127**,161-168 (1969)

[108] D.R. Thompson, M. Lemere and Y.C. Tang, Nucl. Phys. **A286**,53-66 (1977)

[109] I. Reichstein and Y.C. Tang, Nucl. Phys. **A158**, 529-545 (1970)

[110] I. Reichstein and Y.C. Tang, Nucl. Phys. **A139**, 144-148 (1969)

[111] D.R. Thompson, I. Reichstein, W. McClure and Y.C. Tang, Phys. Rev. **183**, 4 (1969)

[112] T. Kaneko and Y.C. Tang, Nucl. Phys. **A548**, 189 - 204 (1992)

[113] H. Kanada, T. Kaneko and Y.C. Tang, Nucl. Phys. **A380**,87-110 (1982)

[114] G. E. Brown and A. D. Jackson, *The Nucleon–Nucleon Interaction* (North-Holland, Amsterdam, 1976).

[115] J. Raynal and J. Revai, Nuovo Cim. **68A**, 612 (1970)

[116] M. Fabre de la Ripelle, The hyperspherical expansion method, *Models and Methods in Few-Body Physics // Springer Lecture Notes in Phys. / Ed. L.S. Ferreira, A.C Fonseca, L. Streit. N.Y.: Springer-Verlag*, **273** 302p

[117] S.A. Sofianos, G.J. Rampho and R.M. Adam, *Physics of Particles and Nuclei*, **40**, 6, 757 - 772 (2009)

[118] Md. A. Khan, Int. J. Mod. Phys. **E 24**, 12 (2015)

[119] Md. A. Khan, Int. J. Mod Phys. **E 23**, 10 (2014)

[120] M. Fabre de la Ripelle and J. Navarro, Ann. Phys. (1979)

[121] F. Pougheon *et al.*, Europhys. Lett. **2**, 505 (1986)

[122] J.D. Stevenson and P.B. Price, Phys. Rev. **C 24**, 2102 (1981)

[123] M. Langevin *et al.*, Phys. Lett. **B 150**, 71 (1985)

[124] P. Descouvemont, Nucl. Phys. **A 675**, 559 (2000)

[125] K. Varga and Y. Suzuki,Phys. Rev. **C 52**, 2885 (1995)

[126] J. Casal *et al.*, Phys. Rev. **C 94**,054622 (2016)

[127] Y. Kucuk and J.A. Tostevin, Phys. Rev. **C 89**, 034607 (2014)

[128] L.H. Thomas, Phys. Rev. **47**, 903 (1935)

[129] Y. Suzuki and K. Varga, *in Stochastic Variational Approach to Quantum-Mechanical Few-Body Problems*, Lecture Notes in Physics, Vol. m54 (Springer-Verlag, Berlin, (1998)

[130] L.V. Grigorenko, N.B. Shulgina and M.V. Zhukov, Phys. Rev. **C 102**,014611 (2020)

[131] S.H Dong and M.C Cruz-Irisson, J. Math. Chem. **50**, 881 (2012)

[132] X.Q Song, C.W Wang and C.S Jia, Chem. Phys. Lett. **673**, 50 (2017)

[133] O.J. Oluwadare, K.J. Oyewumi and T.O. Abiola, Indian J. Phys. **96**, 1921 (2022)